Jyväskylän yliopiston julkaisuarkisto
Jyväskylä University Digital Archive

UNIVERSITY OF JYVÄSKYLÄ

This is an electronic reprint of the original article.
This reprint *may differ* from the original in pagination and typographic detail.

Author(s): Herzan, Andrej; Juutinen, Sakari; Auranen, Kalle; Grahn, Tuomas; Greenlees, Paul; Hauschild, Karl; Jakobsson, Ulrika; Jones, Peter; Julin, Rauno; Ketelhut, Steffen; Leino, Matti; Lopez-Martens, Araceli; Nieminen, Päivi; Nyman, Markus; Peura, Pauli; Rahkila, Panu; Rinta-Antila, Sami; Ruotsalainen, Panu; Sandzelius, Mikael; Sarén, Jan; Scholey, Catherine; Sorri, Juha; Uusitalo, Juha

Title: Detailed spectroscopy of 193Bi

Year: 2015

Version:

Please cite the original version:

Herzan, A., Juutinen, S., Auranen, K., Grahn, T., Greenlees, P., Hauschild, K., Jakobsson, U., Jones, P., Julin, R., Ketelhut, S., Leino, M., Lopez-Martens, A., Nieminen, P., Nyman, M., Peura, P., Rahkila, P., Rinta-Antila, S., Ruotsalainen, P., Sandzelius, M., . . . Uusitalo, J. (2015). Detailed spectroscopy of 193Bi. Physical Review C, 92(4), Article 044310. https://doi.org/10.1103/PhysRevC.92.044310

All material supplied via JYX is protected by copyright and other intellectual property rights, and duplication or sale of all or part of any of the repository collections is not permitted, except that material may be duplicated by you for your research use or educational purposes in electronic or print form. You must obtain permission for any other use. Electronic or print copies may not be offered, whether for sale or otherwise to anyone who is not an authorised user.

Detailed spectroscopy of ^{193}Bi

A. Herzáň,[1] S. Juutinen,[1] K. Auranen,[1] T. Grahn,[1] P. T. Greenlees,[1] K. Hauschild,[1,2] U. Jakobsson,[1,3] P. Jones,[1,4] R. Julin,[1] S. Ketelhut,[1,5] M. Leino,[1] A. Lopez-Martens,[1,2] P. Nieminen,[1,6] M. Nyman,[1,7] P. Peura,[1] P. Rahkila,[1] S. Rinta-Antila,[1] P. Ruotsalainen,[1,5] M. Sandzelius,[1] J. Sarén,[1] C. Scholey,[1] J. Sorri,[1] and J. Uusitalo[1]

[1]*University of Jyvaskyla, Department of Physics, P.O. Box 35, FI-40014 University of Jyvaskyla, Finland*
[2]*CSNSM, IN2P3-CNRS, F-91405 Orsay Campus, France*
[3]*KTH, Department of Physics, SE-10691 Stockholm, Sweden*
[4]*iThemba Laboratory for Accelerator Based Sciences, P.O. Box 722, 7129 Somerset West, South Africa*
[5]*TRIUMF, Westbrook Mall, Vancouver, British Columbia V6T 2A3, Canada*
[6]*Fortum Oyj, Power Division, P.O. Box 100, 00048 Fortum, Finland*
[7]*European Commission, Joint Research Centre, IRMM, Retieseweg 111, B-2440 Geel, Belgium*

(Received 17 June 2015; published 12 October 2015)

An experiment aiming to study shape coexistence in ^{193}Bi has been performed. Due to its transitional character, it has an exceptionally large number of structures identified close to the yrast line. Many new states have been found, significantly extending the previously known level scheme of ^{193}Bi, including several new rotational bands. The $\pi i_{13/2}$ band was extended to $I^\pi = 45/2^+$. The $I^\pi = 31/2^+$ member of the $\pi i_{13/2}$ band was found to de-excite also to a long-lived isomeric state. This isomeric state is located at 2350 keV and has a spin and parity of $29/2^+$. The half-life of the isomeric state was measured to be 85(3) μs and it decays via the emission of an 84 keV $E2$ transition. A level structure feeding this isomeric state was constructed. A low-energy, 49 keV transition has been identified to depopulate the $(29/2^-)$ isomeric state, which places it at an energy 2405 keV in the level scheme. This is the first time such a decay has been observed in the neutron-deficient Bi isotopes. A superdeformed band almost identical to that present in the neighboring isotope ^{191}Bi, based on the 1/2[651] Nilsson orbital, has also been identified.

DOI: 10.1103/PhysRevC.92.044310 PACS number(s): 21.10.Re, 23.20.En, 23.35.+g, 27.80.+w

I. INTRODUCTION

In certain nuclear mass regions, low-lying excited states are associated with a variety of nuclear shapes. One such region, in which coexisting deformed configurations at low excitation energies have been observed, lies close to the proton magic number $Z = 82$ in the neutron midshell region [1,2]. The ^{193}Bi nucleus is in the transitional region between lighter very neutron-deficient odd-A prolate bismuth nuclei [3] and heavier odd-A bismuth isotopes with the absence of any regular bandlike structures for the low-lying states [4–6]. The bismuth nuclei are of interest as they have only one extra proton coupled to the $Z = 82$ proton magic lead core. It is therefore desirable to perform an investigation of shape coexistence and studies of the isomeric states built on multiquasiparticle configurations.

In previous studies [7,8], strongly coupled rotational bands based on the proton 13/2[606] and 7/2[514] Nilsson orbitals have been observed in ^{191,193}Bi nuclei, in contrast to ^{195}Bi, where very limited spectroscopic information exists [9,10]. Irregular bandlike structures built on the $1/2^+$ proton intruder state have been observed in ^{191}Bi and ^{193}Bi. In ^{195}Bi the corresponding state is also known, but the feeding level structure has remained unobserved. An isomeric state with $T_{1/2} = 3$ μs has been reported in ^{193}Bi [7]. Although the depopulating transition was not observed, this was tentatively assigned with a spin and parity of $29/2^-$ based on systematics in heavier odd-mass Bi nuclei [4]. The structure of the isomer is associated with the coupling of an $h_{9/2}$ proton to the 12^+ isomeric state in the ^{192}Pb core. In several odd-A At isotopes, isomeric states with a spin and parity of $29/2^+$ have been identified [11–15] and associated with the coupling of the $h_{9/2}$ proton to the $\pi(h_{9/2}i_{13/2})$ configuration.

Moreover, the search for highly excited superdeformed (SD) bands to better understand the nuclear properties under extreme deformation has turned out to be very successful in this region of the nuclear chart [8,16–20]. Many theoretical calculations [21–23] predict well-defined secondary SD minima persisting in the bismuth and polonium nuclei. Thus far, two SD bands have been reported in the odd-A neighbor ^{191}Bi [8], the lightest Bi isotope in which superdeformation has been experimentally observed.

In the present study, a new high-spin isomeric state with a spin and parity of $29/2^+$ was identified. Both the $29/2^+$ and $29/2^-$ isomers have been connected firmly to the rest of the level scheme. In total, four isomeric states have been observed in ^{193}Bi, with half-lives ranging from a hundred nanoseconds up to a few seconds. We also report on the discovery of one SD band in ^{193}Bi. The similarities between the SD band observed in this work and those seen in ^{191}Bi are emphasized, and an interpretation in terms of a specific proton excitation is presented.

II. EXPERIMENTAL DETAILS

The experiment was carried out at the Accelerator Laboratory of the University of Jyväskylä (JYFL), Finland. The ^{193}Bi nuclei were produced in the fusion-evaporation reaction ^{165}Ho(^{32}S,4n)^{193}Bi, where the $^{32}S^{7+}$ beam, provided by the K-130 cyclotron, was accelerated to an energy of 152 MeV with an average beam current of 17 particle nA (pnA)

 ©2015 American Physical Society

(130 h irradiation time). The self-supporting target was a ^{165}Ho foil with a thickness of 350 μg/cm^2. The reaction products were studied using in-beam γ-ray spectroscopy combined with decay spectroscopy.

The fully digitized JUROGAM II Ge detector array was used to detect prompt γ rays at the target position. The array consisted of 24 clover [24] and altogether 15 Eurogam Phase1 [25] or GASP [26] Compton-suppressed high-hurity germanium (HPGe) detectors. These detectors were instrumented with Lyrtech VHS-ADC cards, which allowed direct digitization of the preamplifier signals. The energies of detected γ rays were determined using a moving window deconvolution (MWD) algorithm [27] implemented in the field-programmable gate array (FPGA) of the analog-to-digital converter (ADC) cards. The total photopeak efficiency of JUROGAM II using the add-back technique was 5.2% at 1.3 MeV. The JUROGAM II array was coupled to the gas-filled recoil separator RITU [28,29] to separate the nuclei of interest from unwanted particles. The ions transported through the separator were subsequently implanted in the GREAT focal plane spectrometer [30] for the identification of fusion products of interest (recoils, Re). When arriving in GREAT, the recoils passed through a multiwire proportional counter (MWPC) and continued to the main instrument of the GREAT spectrometer: two 300 μm thick double-sided silicon strip detectors (DSSD), 40 mm $\times$ 60 mm in size with a 1 mm strip pitch. The DSSD was used for the implantation of recoils and for the detection of their subsequent decays such as α decay in horizontal strips (DSSD-Y side) or internal conversion electrons in vertical strips (DSSD-X side) [30]. To collect the α particles and conversion electrons that have escaped from the DSSD, silicon PIN diode detectors were mounted in a box arrangement upstream from the DSSD. A planar Ge strip detector was mounted directly behind the DSSD to detect low-energy γ rays and x rays. A set of three clover HPGe detectors was added to face the GREAT chamber from the sides and from above to detect high-energy γ rays. All data channels were recorded synchronously using the triggerless total data readout (TDR) [31] data acquisition system. All the events were time-stamped using a 100 MHz clock. The data were analyzed using the recoil-gating, recoil-decay tagging (RDT) [32], and isomer-tagging techniques [33] and processed using the GRAIN [34] and RADWARE [35,36] software packages.

III. RESULTS

The ^{193}Bi nucleus has two α-decaying states: the $9/2^-$ ground state [E_α = 5899(5) keV, I_α = 95.8% and E_α = 6174(5) keV, I_α = 4.2%] and the $1/2^+$ proton intruder state lying at 307 keV [E_α = 6475(5) keV] [37]. The very small α-decay branch of the ground state, b_α = 3.5(15)%, together with its long half-life of 67(3) s [37] makes it difficult to obtain clean recoil-α correlations. On the other hand, the $1/2^+$ intruder state with a total α-decay branch of $b_\alpha = 90^{+10}_{-20}$ % and an α-decay half-life of $T_{1/2}$ = 3.2(6) s [37] enabled us to perform an RDT analysis. An α-particle energy spectrum collected with the DSSD detectors is shown in Fig. 1.

The level scheme presented in the earlier study by Nieminen *et al.* [7] has been extended. Many new states have been found,

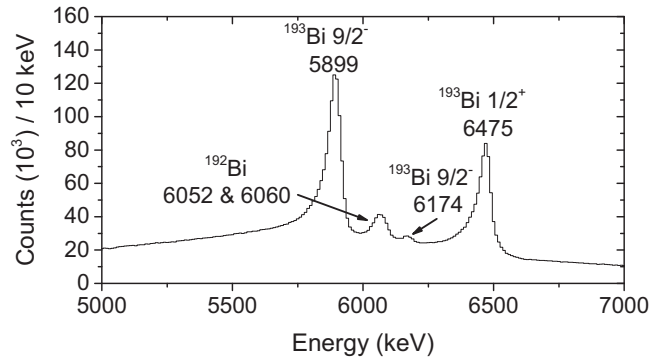

FIG. 1. Energy spectrum of alpha particles (vetoed by MWPC) from the reaction ^{165}Ho(^{32}S,xn)$^{197-x}$Bi collected in DSSDs.

and the related γ-ray transitions are listed in Table I. The ordering of these γ-ray transitions has been established based on a detailed coincidence analysis of γ-γ matrices and a γ-γ-γ cube. As a result, the level scheme shown in Fig. 2 has been constructed.

The values of angular distribution ratios (R_{DCO}) were extracted from two γ-γ matrices, which were formed by sorting recoil-gated prompt coincidence events with (157.6°) vs (all angles) and (75.5°) vs (all angles) combinations. By setting the same energy gates on the (all angles) projection spectrum in both matrices, two coincidence spectra were made representing the aformentioned detection angles. The intensities of the γ-ray transitions of interest were extracted from these spectra and normalized for the detection efficiency. The DCO (directional correlations deexciting oriented states [38]) ratio was calculated using the formula

$$R_{\rm exp} = \frac{I_\gamma(157.6^\circ)}{I_\gamma(75.5^\circ)}.$$

The typical values for stretched dipole and quadrupole transitions are 0.8 and 1.3, respectively. The resulting $R_{\rm exp}$ values with the error estimates are listed in Table I.

The JUROGAM II array was also used to determine the linear polarization of γ-ray transitions (IPDCO, integrated polarizational-directional correlation from oriented nuclei [39]). Two γ-γ matrices were created as follows: The first γ ray corresponds to a single-crystal hit in any detector of the array and the second one to the sum of the energy deposited in two crystals within the same clover detector located either at 75.5° or 104.5° relative to the beam axis. With such a procedure, the matrices contain events with either horizontally or vertically scattered γ rays in a clover (at the angles mentioned above) on one axis and a single-crystal hit on any of the detectors on the other axis. The experimental polarization asymmetry is defined as

$$\Delta_{\rm IPDCO} = \frac{[a(E_\gamma)N_\perp] - N_\parallel}{[a(E_\gamma)N_\perp] + N_\parallel},$$

where $N_\perp$ and $N_\parallel$ denote the number of coincidence counts between the segments of the clover detector in the direction perpendicular and parallel to the emission plane, respectively. The $a(E_\gamma)$ is the normalization factor corresponding to the

TABLE I. Energies E_γ, relative intensities (obtained from JUROGAM II data) I_γ, excitation energies E_i, and initial and final spins I_i^π and I_f^π, respectively, for the γ-ray transitions assigned to ^{193}Bi. Also angular distribution ratios $R_{\rm exp}$, linear polarization asymmetry factors $\Delta_{\rm IPDCO}$, and multipolarities are shown. The intensities have been normalized with respect to the 323.4 keV $15/2^+ \rightarrow 13/2^+$ transition. The statistical error of about 0.3 keV should be added to the fitting errors given for most of the transitions listed in the first column.

E_γ (keV)	I_γ (%)	E_i (keV)	I_i^π	I_f^π	$R_{\rm exp}$	$\Delta_{\rm IPDCO}$	Multipolarity
Band 1							
90.0(5)	22(2)	2964	$31/2^+$	$29/2^+$			$M1$
117.1(1)	15.9(6)	2874	$29/2^+$	$27/2^+$	0.69(4)		$M1$
153.6(1)	29(1)	3118	$33/2^+$	$31/2^+$	0.78(4)		$M1$
164.5(1)	5.3(3)	2757	$27/2^+$	$25/2^+$			$M1$
203.9(1)	40(2)	3322	$35/2^+$	$33/2^+$	0.63(3)	−0.13(1)	$M1$
220.4(1)	47(2)	2757	$27/2^+$	$25/2^+$	0.73(2)	−0.073(4)	$M1$
239.8(1)	30(1)	3561	$37/2^+$	$35/2^+$	0.60(3)	−0.016(13)	$M1$
276.5(1)	22.9(9)	3839	$39/2^+$	$37/2^+$	0.76(3)	−0.06(1)	$M1$
294.4(1)	5.9(4)	4588					
299.2(1)	258(8)	1228	$17/2^+$	$15/2^+$	0.68(2)	−0.032(1)	$M1$
299.8(1)	17.0(9)	4139	$41/2^+$	$39/2^+$	0.6(1)		$M1$
315.2(1)	63(2)	2536	$25/2^+$	$23/2^+$	0.79(4)		$M1$
323.4(1)	1000(57)	929	$15/2^+$	$13/2^+$	0.74(4)	−0.012(1)	$M1$
327.4(1)	196(6)	1556	$19/2^+$	$17/2^+$	0.68(2)	−0.004(1)	$M1$
330.3(2)	4.1(4)	4469	$43/2^+$	$41/2^+$	0.82(16)		$M1$
345.7(1)	86(3)	2221	$23/2^+$	$21/2^+$	0.68(2)	−0.059(6)	$M1$
356.7(2)	2.5(3)	4826	$45/2^+$	$43/2^+$	0.7(2)		$M1$
443.8(4)	5.6(6)	3561	$37/2^+$	$33/2^+$			$E2$
454.9(2)	1.9(4)	4294		$39/2^+$			
516.4(2)	6.3(8)	3839	$39/2^+$	$35/2^+$	1.6(5)		$E2$
576.6(6)	6(1)	4139	$41/2^+$	$37/2^+$	0.85(25)		$E2$
604.7(1)[a]		605	$13/2^+$	$9/2^-$			$M2$
622.4(1)	121(5)	1228	$17/2^+$	$13/2^+$	1.30(16)	0.086(10)	$E2$
626.2(1)	102(4)	1556	$19/2^+$	$15/2^+$	1.48(6)	0.094(9)	$E2$
630.4(4)	1.9(3)	4469	$43/2^+$	$39/2^+$			$E2$
646.9(1)	108(4)	1875	$21/2^+$	$17/2^+$	1.47(6)	0.091(4)	$E2$
660.7(1)	74(3)	2536	$25/2^+$	$21/2^+$	1.15(14)	0.060(3)	$E2$
665.2(1)	80(3)	2221	$23/2^+$	$19/2^+$	1.2(1)	0.072(7)	$E2$
Band 2							
124.6(1)	7.9(4)	2587	$25/2^-$	$23/2^-$			$M1$
134.7(1)	12.9(5)	2722	$27/2^-$	$25/2^-$	0.62(9)		$M1$
155.2(1)	7.0(5)	620	$11/2^-$	$9/2^-$			$M1$
186.3(1)	24(1)	465	$9/2^-$	$7/2^-$	0.52(14)		$M1$
198.2(1)	29(2)	818	$13/2^-$	$11/2^-$	0.73(7)		$M1$
206.3(1)	12.6(6)	2928	$(29/2^-)$	$27/2^-$			$(M1)$
245.2(1)	42(2)	1415	$17/2^-$	$15/2^-$	0.67(5)	−0.12(2)	$M1$
255.1(1)	18.3(8)	2049	$21/2^-$	$19/2^-$	0.66(10)		$M1$
278.5(1)	103(4)	279	$7/2^-$	$9/2^-$	0.9(1)		$M1$
341.1(2)	5.4(7)	620	$11/2^-$	$7/2^-$			$E2$
352.1(1)	154(5)	1170	$15/2^-$	$13/2^-$	0.72(6)	−0.036(4)	$M1$
353.1(2)	7.7(6)	818	$13/2^-$	$9/2^-$			$E2$
379.4(1)	84(3)	1794	$19/2^-$	$17/2^-$	0.64(4)	−0.050(1)	$M1$
414.3(1)	20.3(9)	2463	$23/2^-$	$21/2^-$	0.43(6)	(−0.12(2))	$M1$
465.2(6)	4(1)	465	$9/2^-$	$9/2^-$			$(M1)$
538.4(1)	29(2)	2587	$25/2^-$	$21/2^-$	1.40(17)	0.07(1)	$E2$
550.0(1)	173(6)	1170	$15/2^-$	$11/2^-$	1.27(10)	0.06(2)	$E2$
597.0(1)	260(9)	1415	$17/2^-$	$13/2^-$	1.05(10)	0.016(1)	$E2$
619.7(1)	358(29)	620	$11/2^-$	$9/2^-$	0.85(9)	−0.059(6)	$M1$
624.3(1)	136(5)	1794	$19/2^-$	$15/2^-$	1.20(5)	0.024(2)	$E2$
634.1(1)	148(5)	2049	$21/2^-$	$17/2^-$	1.57(9)	0.07(1)	$E2$
668.9(1)	50(2)	2463	$23/2^-$	$19/2^-$	1.48(12)	0.103(11)	$E2$
817.9(1)	377(18)	818	$13/2^-$	$9/2^-$	1.22(4)	0.039(3)	$E2$

TABLE I. (*Continued.*)

E_γ (keV)	I_γ (%)	E_i (keV)	I_i^π	I_f^π	$R_{\rm exp}$	$\Delta_{\rm IPDCO}$	Multipolarity
Band 3							
103.4(1)	9.7(5)	2194	$19/2^-$	$17/2^-$	0.41(3)		$M1$
143.0(1)	34(2)	2337	$21/2^-$	$19/2^-$	0.95(5)		$M1$
146.8(1)	31(1)	2484	$23/2^-$	$21/2^-$	0.83(4)		$M1$
185.5(1)	36(2)	2670	$25/2^-$	$23/2^-$	0.71(6)		$M1$
204.4(1)	10.5(5)	4213	$(37/2^-)$	$35/2^-$	0.67(4)		$M1$
212.7(1)	5.1(4)	4009	$35/2^-$	$33/2^-$	0.76(5)		$M1$
231.9(4)	1.2(3)	4242	$(37/2^-)$	$35/2^-$			$(M1)$
252.5(1)	43(2)	2922	$27/2^-$	$25/2^-$	0.61(6)	−0.008(1)	$M1$
263.1(1)	6.2(4)	4060	$(35/2^-)$	$33/2^-$	0.67(5)		$M1$
278.6(1)	41(2)	3201	$29/2^-$	$27/2^-$	0.92(8)	−0.053(4)	$M1$
284.0(1)	5.9(5)	2194	$19/2^-$	$17/2^-$			$M1$
295.7(1)	24(1)	3497	$31/2^-$	$29/2^-$	0.57(5)	−0.096(6)	$M1$
298.8(1)	32(2)	3796	$33/2^-$	$31/2^-$	0.60(5)	−0.093(6)	$M1$
(334.7(3))	2.8(4)	2922	$27/2^-$	$25/2^-$			$M1$
438.1(4)	2.9(6)	2922	$27/2^-$	$23/2^-$			$E2$
512.7(1)	8.4(5)	4009	$35/2^-$	$31/2^-$			$E2$
530.9(2)	7.5(6)	3201	$29/2^-$	$25/2^-$	2.1(3)		$E2$
574.3(1)	10.9(7)	3497	$31/2^-$	$27/2^-$	2.2(3)	0.105(14)	$E2$
595.9(1)	21(1)	3796	$33/2^-$	$29/2^-$			$E2$
631.4(1)	13.3(8)	2194	$19/2^-$	$15/2^-$			$E2$
Band 4							
253.1(1)	8.8(6)	916	$11/2^-$	$9/2^-$		−0.14(2)	$M1$
313.3(1)	11.5(7)	1563	$15/2^-$	$13/2^-$	0.61(8)	−0.049(9)	$M1$
333.7(1)	22(1)	1250	$13/2^-$	$11/2^-$	0.66(10)		$M1$
347.6(2)	4.5(6)	1910	$17/2^-$	$15/2^-$			$(M1)$
383.8(1)	43(2)	662	$9/2^-$	$7/2^-$	0.91(5)		$M1$
450.6(1)	12.5(8)	916	$11/2^-$	$9/2^-$		−0.035(4)	$M1$
587.0(1)	19(1)	1250	$13/2^-$	$9/2^-$			$(E2)$
636.7(1)	22(2)	916	$11/2^-$	$7/2^-$	1.15(7)		$E2$
647.3(1)	43(2)	1563	$15/2^-$	$11/2^-$	1.53(16)		$E2$
661.1(2)	10.2(9)	1910	$17/2^-$	$13/2^-$			$(E2)$
661.6(3)	19(3)	662	$9/2^-$	$9/2^-$	0.60(11)		$M1+E2$
677.9(4)	10.0(8)	2241	$19/2^-$	$15/2^-$	1.41(23)		$E2$
784.5(2)	8.8(7)	1250	$13/2^-$	$9/2^-$	1.81(22)		$E2$
844.0(1)	17(2)	1910	$17/2^-$	$13/2^-$			$(E2)$
915.5(1)	61(4)	916	$11/2^-$	$9/2^-$	0.45(8)	0.012(2)	$M1+E2$
Band 5							
48.8(5)[a]		2405	$(29/2^-)$	$25/2^-$			$(E2)$
261.3(1)	7.6(5)	3710	$(37/2^-)$	$(35/2^-)$	0.81(14)		$M1$
289.5(1)	16.5(8)	3448	$(35/2^-)$	$(33/2^-)$	0.93(9)	−0.033(5)	$M1$
318.8(1)	6.3(5)	4029	$(39/2^-)$	$(37/2^-)$			$(M1)$
355.3(1)	32(1)	3159	$(33/2^-)$	$(31/2^-)$	0.80(7)	−0.06(2)	$M1$
386.4(3)	2.0(3)	3670	$(37/2^-)$	$(33/2^-)$	1.32(24)		$E2$
398.8(1)	55(2)	2804	$(31/2^-)$	$(29/2^-)$	0.61(6)	−0.016(5)	$M1$
466.2(3)	1.9(3)	3750		$(33/2^-)$			
478.5(1)	20(1)	3282	$(33/2^-)$	$(31/2^-)$	0.63(9)		$M1$
550.6(2)	4.9(7)	3710	$(37/2^-)$	$(33/2^-)$	1.5(2)		$E2$
580.2(3)	3.3(5)	4029	$(39/2^-)$	$(35/2^-)$			$(E2)$
644.1(4)	3.0(7)	3448	$(35/2^-)$	$(31/2^-)$			$(E2)$
753.9(2)	12.7(14)	3159	$(33/2^-)$	$(29/2^-)$			$(E2)$
879.0(5)	5.8(8)	3282	$(33/2^-)$	$(29/2^-)$			$(E2)$
Band 6							
190.1(1)	4.3(3)	1205	$(9/2^+)$	$(7/2^+)$			$(M1)$
200.2(1)	50(2)	507	$3/2^+$	$1/2^+$	0.78(7)		$M1$
229.3(1)	16.2(8)	736	$5/2^+$	$3/2^+$	0.94(11)	−0.05(3)	$M1$

TABLE I. (*Continued.*)

E_γ (keV)	I_γ (%)	E_i (keV)	I_i^π	I_f^π	R_{exp}	Δ_{IPDCO}	Multipolarity
278.9(7)	1.8(7)	1015	$(7/2^+)$	$5/2^+$			$(M1)$
356.4(5)	1.1(3)	1322					
429.0(2)	13(2)	736	$5/2^+$	$1/2^+$			$E2$
433.0(1)	19.0(9)	1638	$(13/2^+)$	$(9/2^+)$			$(E2)$
459.5(2)	5.2(5)	966		$3/2^+$			
469.3(1)	14.6(8)	1205	$(9/2^+)$	$5/2^+$			$(E2)$
503.1(2)	4.4(6)	2141	$(17/2^+)$	$(13/2^+)$			$(E2)$
504.1(2)	5.8(8)	1519	$(11/2^+)$	$(7/2^+)$			$(E2)$
508.2(1)	35(2)	1015	$(7/2^+)$	$3/2^+$	0.95(12)		$(E2)$
Group A							
357.0(2)	5.6(5)	2894	$(25/2^+)$	$25/2^+$	0.82(7)	−0.178(14)	$(M1)$
371.0(1)	8.1(5)	2592	$25/2^+$	$23/2^+$			$M1$
542.2(3)	3.2(6)	2764	$25/2^+$	$23/2^+$	0.74(9)		$M1$
672.5(1)	13.9(8)	2894	$(25/2^+)$	$23/2^+$	0.86(6)	0.010(1)	$(M1)$
716.3(1)	27(1)	2592	$25/2^+$	$21/2^+$	1.33(8)	0.12(1)	$E2$
736.1(1)	12.8(7)	2957	$25/2^{(+)}$	$23/2^+$	0.74(9)		$(M1/E1)$
887.7(1)	10.8(7)	2764	$25/2^+$	$21/2^+$	1.9(4)		$E2$
929.6(1)	22(2)	1859	$(17/2^+)$	$15/2^+$	0.48(7)	0.13(2)	$(M1+E2)$
Group B							
212.3(2)	3.8(4)	2434	$23/2^+$	$23/2^+$			$M1$
276.0(1)	8.7(6)	2710	$(25/2^+)$	$23/2^+$			$(M1)$
371.7(2)	6.7(7)	2323	$(21/2^+)$	$19/2^+$	0.61(9)		$M1$
375.4(1)	18.9(9)	2434	$23/2^+$	$21/2^+$	0.84(12)		$M1$
435.7(1)	41(2)	1951	$19/2^+$	$17/2^+$	0.58(6)	−0.005(1)	$M1$
488.3(2)	7.4(6)	2710	$(25/2^+)$	$23/2^+$	0.44(5)		$M1+E2$
502.5(1)	41(2)	2058	$21/2^+$	$19/2^+$	0.62(5)		$M1$
534.3(3)	5.5(9)	2049	$(21/2^+)$	$17/2^+$	1.10(8)		$E2$
543.2(1)	15.0(9)	2058	$21/2^+$	$17/2^+$	1.28(13)		$E2$
557.5(2)	7.1(7)	2434	$23/2^+$	$21/2^+$			$(M1)$
585.3(1)	86(3)	1515	$17/2^+$	$15/2^+$	0.66(3)	−0.04(1)	$M1$
651.5(4)	3.3(7)	2710	$(25/2^+)$	$21/2^+$			$(E2)$
721.6(1)	21(1)	1951	$19/2^+$	$17/2^+$	0.63(6)		$M1$
807.3(2)	10.1(9)	2323	$(21/2^+)$	$17/2^+$	0.83(19)		$(E2)$
908.7(1)	74(4)	1515	$17/2^+$	$13/2^+$	1.30(12)	0.056(12)	$E2$
1021.2(1)	19(1)	1951	$19/2^+$	$15/2^+$			$(E2)$
Group C							
(18.7(5))[b]	0.44(3)	2129	$21/2^+$	$19/2^+$			$M1$
137.1(1)	8.6(5)	2266	$25/2^+$	$21/2^+$	1.38(12)		$E2$
137.6(1)	10.0(5)	1673	$17/2^+$	$15/2^+$	0.77(8)		$M1$
149.8(1)	11.1(6)	2279	$25/2^+$	$21/2^+$	1.32(17)		$E2$
159.3(1)	5.6(4)	1673	$17/2^+$	$17/2^+$	1.08(15)		$M1+E2$
188.3(1)	10.1(8)	1117	$13/2^+$	$15/2^+$			$(M1)$
268.9(1)	5.3(3)	2987	$29/2^+$	$27/2^+$	0.38(6)	−0.048(6)	$M1$
278.1(2)	5.0(5)	2997	$29/2^+$	$27/2^+$	0.51(6)	−0.23(3)	$M1$
299.4(4)	4(1)	1117	$13/2^+$	$13/2^-$			$E1$
381.0(2)	13(1)	2510	$23/2^+$	$21/2^+$	0.98(12)	−0.27(4)	$M1$
436.2(1)	77(3)	2110	$19/2^+$	$17/2^+$	0.7(1)	−0.11(2)	$M1$
445.4(2)	10.6(8)	1673	$17/2^+$	$17/2^+$			$M1$
452.2(1)	14.9(7)	2719	$27/2^+$	$25/2^+$	0.8(1)		$M1$
455.4(1)	61(3)	2129	$21/2^+$	$17/2^+$	0.98(20)	0.119(14)	$E2$
469.5(1)	16(1)	1536	$15/2^+$	$13/2^-$	0.80(16)		$E1$
497.5(2)	13(1)	1117	$13/2^+$	$11/2^-$	0.85(12)	−0.053(9)	$E1$
504.0(1)	38(2)	1673	$17/2^+$	$15/2^-$	0.80(6)	0.15(1)	$E1$
511.3(1)	76(7)	1117	$13/2^+$	$13/2^+$	0.93(8)	−0.16(2)	$M1+E2$
556.4(1)	50(2)	1673	$17/2^+$	$13/2^+$	1.37(9)		$E2$
(567.5(1))	8.4(5)	3564	$(31/2^+)$	$29/2^+$			$(M1)$

TABLE I. (*Continued.*)

E_γ (keV)	I_γ (%)	E_i (keV)	I_i^π	I_f^π	$R_{\rm exp}$	$\Delta_{\rm IPDCO}$	Multipolarity
576.2(2)	6.1(5)	3564	$(31/2^+)$	$29/2^+$	0.85(19)		$M1$
695.1(1)	13.1(9)	2110	$19/2^+$	$17/2^-$	1.47(21)		$E1$
717.9(1)	40(2)	1536	$15/2^+$	$13/2^-$	1.02(20)	0.10(1)	$E1$
(721.1(2))	7.9(6)	2987	$27/2^-$	$23/2^-$			$(E2)$
744.7(2)	11.5(9)	1673	$17/2^+$	$15/2^+$	0.79(14)		$M1$
881.3(2)	13(1)	2110	$19/2^+$	$17/2^+$	0.79(13)		$M1$
930.0(1)	58(4)	1536	$15/2^+$	$13/2^+$	0.89(9)	−0.18(2)	$M1$
1067.8(1)	43(3)	1673	$17/2^+$	$13/2^+$	1.08(15)	0.07(3)	$E2$
Group D							
295.1(5)	1.9(5)	2724	$25/2^-$	$23/2^-$			$M1$
459.2(2)	7.7(7)	2253		$19/2^-$			
634.3(1)	34(2)	2428	$23/2^-$	$19/2^-$	1.35(7)		$E2$
654.1(3)	4.5(7)	2448		$19/2^-$			
674.6(1)	23(1)	2724	$25/2^-$	$21/2^-$	1.6(3)		$E2$
726.0(2)	7.9(6)	2776		$21/2^-$			
731.4(1)	15.4(9)	2526	$23/2^-$	$19/2^-$	1.33(23)	0.08(1)	$E2$
784.0(1)	14.2(8)	2578	$23/2^-$	$19/2^-$	1.25(14)		$E2$
839.2(1)	29.6(14)	2254	$(19/2^-)$	$17/2^-$			$(E2)$
Group E							
84.0(5)[a]		2350	$29/2^+$	$25/2^+$			$E2$
158.5(3)	2.5(4)	3118	$33/2^+$	$31/2^+$			$M1$
229.4(3)	1.4(3)	4576		$37/2^-$			$(M1)$
271.9(5)	0.9(3)	4544		$(37/2^+)$			
323.6(2)	5.5(6)	4900					
345.4(1)	11(1)	3304	$33/2^+$	$31/2^+$	0.66(9)		$M1$
386.5(4)	1.8(4)	4272	$(37/2^+)$	$35/2^+$			$(M1)$
390.5(2)	10.4(9)	3350	$33/2^+$	$31/2^+$	0.92(14)		$M1$
512.3(1)	25(2)	3817	$35/2^-$	$33/2^+$	0.73(12)	0.080(14)	$E1$
528.6(1)	8.6(6)	4346	$37/2^-$	$35/2^-$	<1		$M1$
535.0(5)	1.5(5)	3639					
582.1(2)	9.6(9)	3886	$35/2^+$	$33/2^+$	0.9(2)		$M1+E2$
606.5(3)	8(1)	3910		$33/2^+$			
609.1(1)	39(2)	2959	$31/2^+$	$29/2^+$	0.88(13)	−0.017(4)	$M1$
614.0(1)	46(3)	2964	$31/2^+$	$29/2^+$	0.7(1)	−0.07(2)	$M1$
619.9(3)	5.8(9)	3970	$37/2^+$	$33/2^+$	1.18(12)	0.13(2)	$E2$
627.5(4)	0.7(6)	3977		$33/2^+$			
661.3(4)	2.2(5)	4284					
664.0(1)	16(1)	3623		$31/2^+$			
677.2(7)	0.7(3)	4962					
(718.4(6))	0.9(3)	5679					
(725.5(9))	1.0(6)	4030		$33/2^+$			
754.0(5)	16.2(8)	3104		$29/2^+$			
927.9(4)	1.9(4)	3886	$35/2^+$	$31/2^+$			$E2$
954.7(1)	44(6)	3304	$33/2^+$	$29/2^+$	1.31(18)	0.060(3)	$E2$
967.7(3)	2.8(4)	4272	$(37/2^+)$	$33/2^+$			$(E2)$
Group F							
232.1(3)	1.4(3)	2091	$17/2^-$	$15/2^-$			$M1$
242.9(2)	5.5(4)	2194	$19/2^-$	$19/2^+$			$E1$
328.2(3)	4.5(7)	2091	$17/2^-$	$(15/2^-)$			$(M1)$
351.1(1)	2.2(6)	1521	$13/2^-$	$15/2^-$	0.99(9)		$M1$
352.4(2)	5.3(6)	2091	$17/2^-$	$17/2^-$			$(M1)$
365.1(2)	4.2(4)	2722	$27/2^-$	$25/2^-$	0.86(16)		$M1$
435.6(1)	10.1(7)	2484	$23/2^-$	$21/2^-$	0.89(16)		$M1$
446.8(1)	26(2)	1067	$13/2^-$	$11/2^-$	0.85(11)	−0.09(1)	$M1$
(455.1(5))	1.4(6)	1521	$13/2^-$	$13/2^-$			$(M1)$
528.2(2)	4.8(5)	2091	$17/2^-$	$15/2^-$	0.74(10)		$M1$

TABLE I. (*Continued.*)

E_γ (keV)	I_γ (%)	E_i (keV)	I_i^π	I_f^π	R_{exp}	Δ_{IPDCO}	Multipolarity
567.0(1)	23(2)	1737	$17/2^-$	$15/2^-$	0.83(8)	−0.155(14)	$M1$
569.4(1)	31(2)	2091	$17/2^-$	$13/2^-$	1.32(12)		$E2$
605.2(2)	12(1)	1521	$13/2^-$	$11/2^-$	0.95(13)		$M1+E2$
619.9(3)	11(2)	2711		$17/2^-$			
670.3(1)	25(2)	1737	$17/2^-$	$13/2^-$	1.85(22)		$E2$
679.2(1)	24(1)	2194	$19/2^-$	$17/2^+$	0.8(2)	0.15(2)	$E1$
689.6(1)	14.2(7)	2484	$23/2^-$	$19/2^-$	1.45(30)		$E2$
793.5(2)	9(1)	1860	$15/2^-$	$13/2^-$	0.64(10)		$M1$
862.4(1)	16.3(8)	2091	$17/2^-$	$17/2^+$	0.92(8)	0.040(5)	$E1$
901.7(1)	33(2)	1521	$13/2^-$	$11/2^-$	0.7(1)	0.127(14)	$M1+E2$
913.4(3)	5.7(9)	1980		$13/2^-$			
920.9(1)	33(2)	2091	$17/2^-$	$15/2^-$	0.77(8)	−0.12(3)	$M1$
1023.6(2)	9.5(6)	2091	$17/2^-$	$13/2^-$			$E2$
1066.6(1)	104(10)	1067	$13/2^-$	$9/2^-$	1.37(20)		$E2$
1156.8(3)	5(2)	1763	$(15/2^-)$	$13/2^+$			$(E1)$
1272.8(1)	15.3(8)	2091	$17/2^-$	$13/2^-$	1.28(24)		$E2$
Other transitions							
(97.5)[c]	9(1)						
146.0(5)[d]	4.1(3)						
289.0(5)[e]	9(3)						
307.4(1)	27(1)	2356	$25/2^-$	$21/2^-$	1.28(13)	−0.002(1)	$E2$
319.8(1)	125(4)	1875	$21/2^+$	$19/2^+$	0.60(2)	−0.039(2)	$M1$
352.3(1)	13.3(10)	1610	$(13/2^-)$	$(11/2^-)$	0.73(16)	−0.023(7)	$M1$
363.4(2)	9.5(9)	642	$7/2^-$	$7/2^-$	1.16(11)		$M1$
(388.2(5))	1.2(3)	3220		$29/2^-$			
393.4(1)[f]	27(1)	1652	$(15/2^-)$	$(11/2^-)$	1.26(16)		$(E2)$
394.0(1)[f]	8.3(5)	2046	$(19/2^-)$	$(15/2^-)$	1.26(16)	−0.076(11)	$(E2)$
436.3(3)	2.7(4)	2046	$(19/2^-)$	$(15/2^-)$	1.5(5)		$(E2)$
444.0(5)[d]	4.5(3)						
476.0(1)	10.5(5)	2832	$29/2^-$	$25/2^-$	1.2(2)		$E2$
501.5(1)	9.7(5)	2547	$(21/2^-)$	$(19/2^-)$	0.9(1)	−0.053(8)	$M1$
535.2(1)	17.8(8)	2757	$27/2^+$	$23/2^+$	1.4(2)		$E2$
571.1(2)	4.4(4)	3119	$(23/2^-)$	$(21/2^-)$	0.6(1)		$(M1)$
638.1(3)	3.1(5)	1258	$(11/2^-)$	$11/2^-$			$(M1)$
647.3(1)	43(2)	1563	$15/2^-$	$11/2^-$	1.53(16)		$E2$
793.1(1)	6.2(7)	1258	$(11/2^-)$	$9/2^-$	0.44(5)		$(M1+E2)$
1258.1(1)	19(2)	1258	$(11/2^-)$	$9/2^-$	0.82(11)		$(M1)$

[a]A γ-ray transition depopulating the isomeric state.
[b]The energy of this transition is obtained from the difference of the level energies of the $19/2^+$ and $21/2^+$ members of Group C.
[c]Seen in coincidence with the 143.0, 146.8, 185.5, 252.5, and 278.6 keV transitions in the prompt γ-ray spectra.
[d]Seen in delayed coincidence with the members of Band 2 and the 307 keV transition.
[e]Seen in coincidence with the members of Band 1 in the prompt γ-ray spectra.
[f]The DCO and IPDCO value applies for both transitions. The ordering of these two transitions is not clear as they are too close to each other in the coincidence γ-ray spectrum.

asymmetry of the JUROGAM II array and is defined as

$$a(E_\gamma) = \frac{N_\parallel(\text{unpolarized})}{N_\perp(\text{unpolarized})},$$

where $N_\parallel$(unpolarized) and $N_\perp$(unpolarized) have the similar meanings as $N_\parallel$ and $N_\perp$ given above but they are obtained in a case of unpolarized radiation. The normalization factor a is a function of γ-ray energy and has been obtained from the measurement with a standard ^{152}Eu radioactive source. Figure 3 shows the variation of a with E_γ. As one can see, the value of a is very close to unity and varies only minimally with the energy, therefore showing that the clovers are nearly symmetric. The number of horizontally ($N_\perp$) and vertically ($N_\parallel$) scattered events for a given γ ray was obtained by setting gates on coincident single-crystal hit γ-ray transitions in the two asymmetric matrices. Based on the experimental results obtained in this work using the JUROGAM II array, stretched magnetic transitions have a value of $\Delta_{IPDCO} \sim -0.1$ and those of stretched electric transitions of ~ 0.1.

To determine the polarization sensitivity Q of the JUROGAM II array, the linear polarization P of stretched $M1$ and $E2$ transitions have been calculated. Consequently, the relation

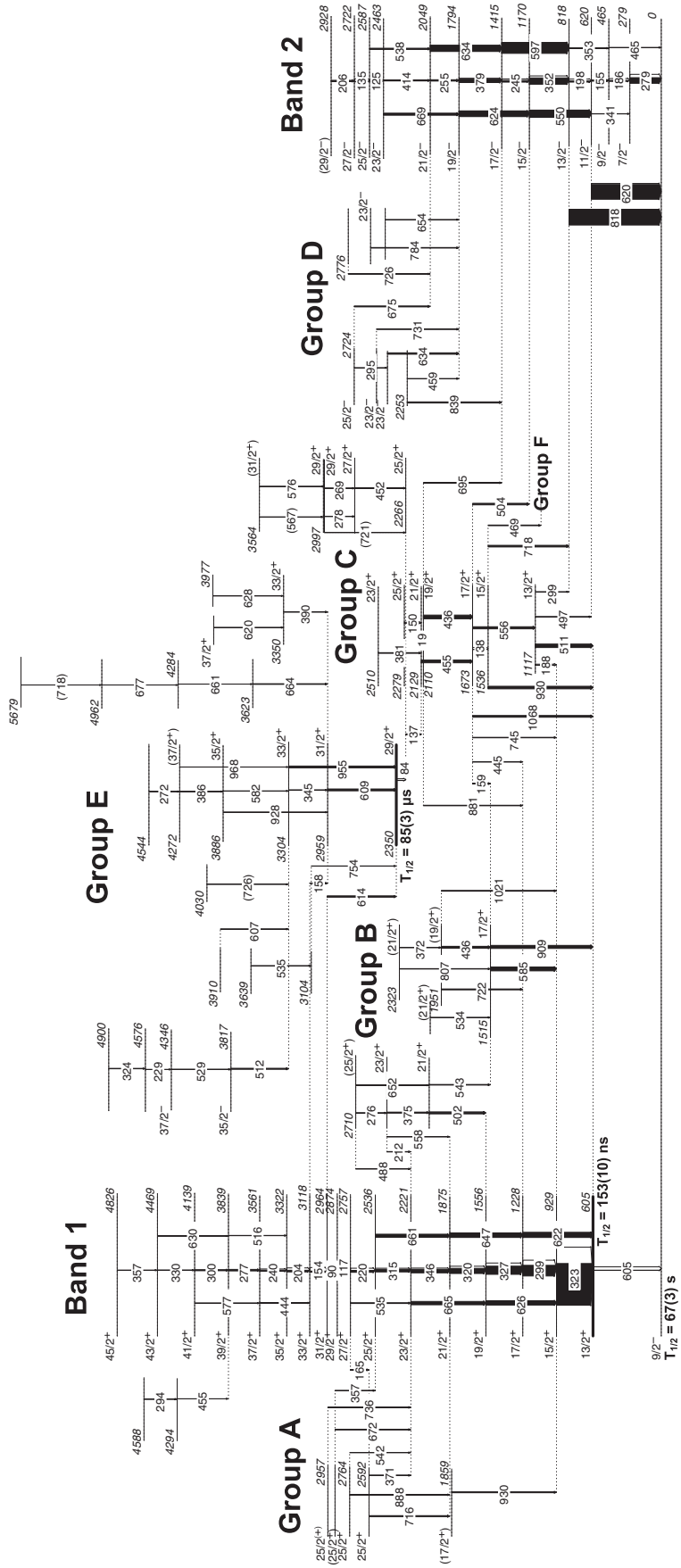

FIG. 2. The level scheme of ^{193}Bi.

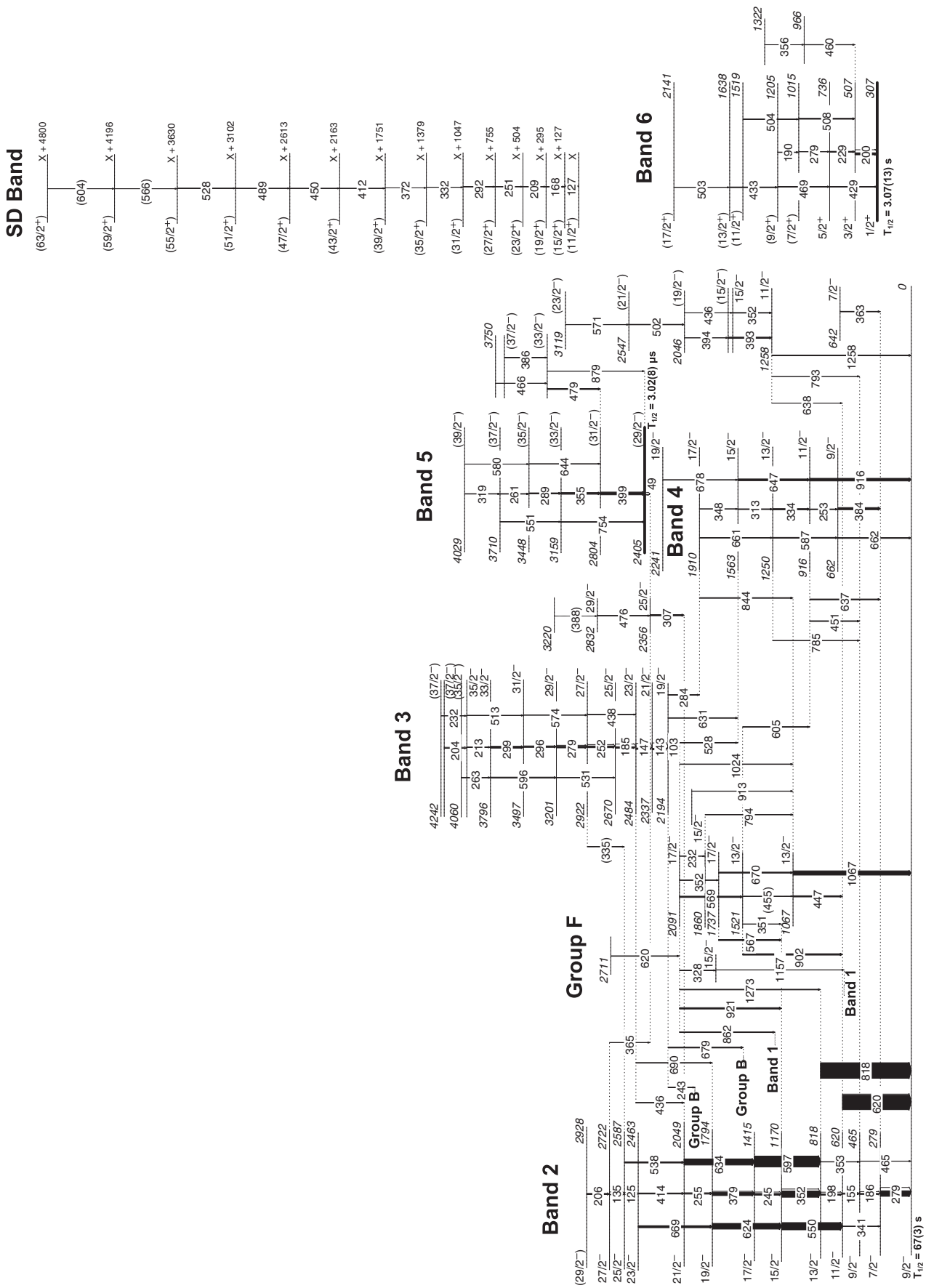

FIG. 2. (Continued.)

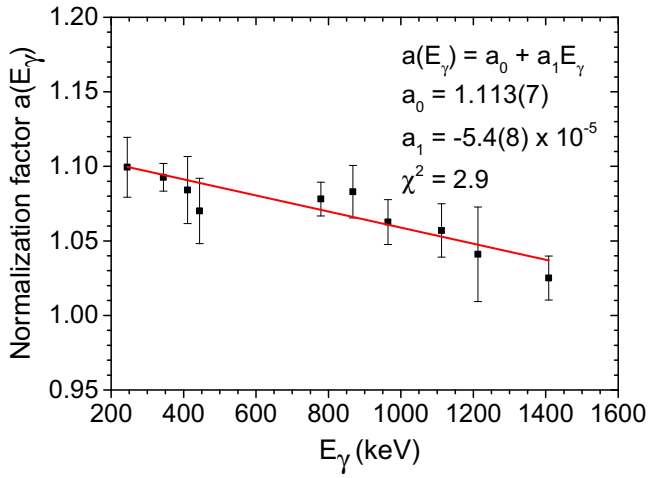

FIG. 3. (Color online) Normalization factor a in the linear polarization measurements as a function of γ-ray energy (E_γ) for the JUROGAM II array.

A = Q P can be used, where $A = \Delta_{\mathrm{IPDCO}}$. The experimental values of $Q(E_\gamma)$ are shown in Fig. 4.

The coefficients p_0 and p_1 were determined by a least-square fit to calculated values of Q using the function for effective polarization sensitivity, usually given as

$$Q = Q_{\mathrm{point}}(p_0 + p_1 E_\gamma).$$

The Klein-Nishina formula [40] gives

$$Q_{\mathrm{point}} = \frac{1+\alpha}{1+\alpha+\alpha^2},$$

where $\alpha = \frac{E_\gamma}{m_e c^2}$ and m_e is the electron rest mass.

A. Spherical and oblate states

The present results, utilizing γ-γ and γ-γ-γ coincidences and energy-sum arguments, support the previously reported level scheme. The present study allowed the knowledge of this nucleus to be extended considerably and resulted in a rather complicated level scheme.

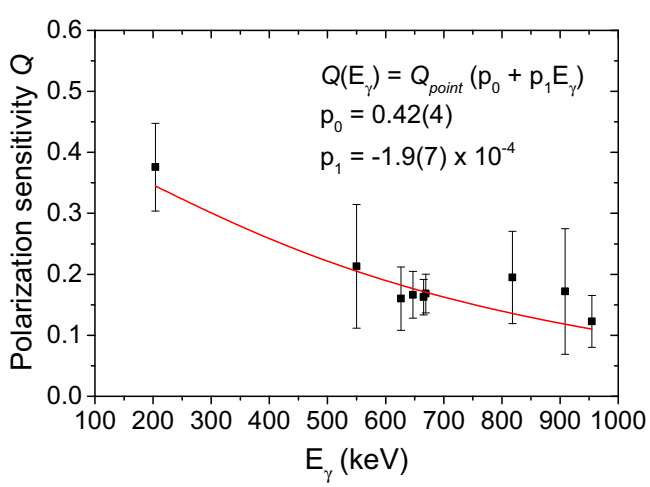

FIG. 4. (Color online) Polarization sensitivity of the JUROGAM II array. The solid line is the fit to our data.

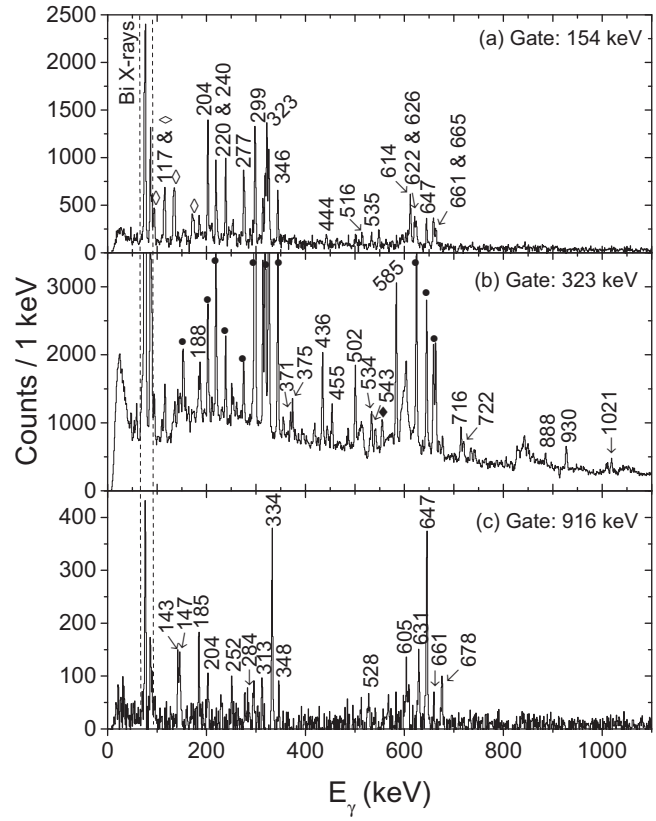

FIG. 5. (a) An energy spectrum of prompt γ rays gated on the 154 keV transition depopulating the $I^\pi = 33/2^+$ member of Band 1. The peak assigned with energy 323 keV is a quadruplet consisting of 315, 320, 323, and 327 keV γ rays. (b) 323.4 keV-gated γ-ray spectrum showing the main part of those γ-ray transitions feeding Band 1. (c) The spectrum of prompt γ rays gated on the 916 keV transition. Peaks marked with an empty diamond symbol belong to ^{165}Ho. Circle symbols refer to γ-ray transitions of Band 1. Full diamonds denote the other γ-ray transitions belonging to ^{193}Bi.

1. Band 1

The $13/2^+$ bandhead of Band 1 has a half-life of 153(10) ns [7]. The band structure feeding the isomeric $13/2^+$ state (Band 1) was previously observed up to $I^\pi = (29/2^+)$, where the statistics did not allow firm assignment of the two uppermost states. In the present study, Band 1 was extended up to $I^\pi = 45/2^+$ at an energy of 4.826 MeV [for corresponding transitions see Fig. 5(a)]. Band 1 undergoes a sharp band-crossing above $I^\pi = 25/2^+$. Experimental intensity ratios R_{exp} and linear polarization asymmetry factors, listed in Table I, support the previously assigned $M1$ and $E2$ character for the transitions reported by Nieminen *et al.* [7] and extend this information up to the topmost members of the band. A γ-ray spectrum gated on the 154 keV transition, placed just above the band crossing, is shown in Fig. 5(a). A strong γ-ray peak with an energy of 614 keV, which does not belong to Band 1,

appears in this spectrum. This transition provides a connection to another level structure (Group E).

States with positive parity in Groups A, B, and C de-excite to the members of Band 1. Most of these transitions can be immediately seen when gating on the 323 keV γ-ray transition in the prompt γ-γ coincidence matrix [see Fig. 5(b)]. In total, more than 20 γ-ray transitions have been found to originate from the states of positive parity and feed Band 1 up to spin 25/2 (see Fig. 2).

2. Band 2

In the previous study by Nieminen *et al.* [7] the negative parity Band 2 was deduced up to $I^\pi = (25/2^-)$ with only tentative spin assignment for the uppermost states. Here, gating on the strongest transitions of Band 2 (see Fig. 2) helped not only to extend this band to higher spin, $I^\pi = 29/2^-$, by the 125, 135, and 206 keV transitions, but also to reveal the bandhead for the first time. The population of the bandhead from the members of the band is however weak, since the main decay out of the band proceeds via the emission of two intense higher energy γ rays with energies of 620 and 818 keV, depopulating the $11/2^-$ and $13/2^-$ states, respectively. Based on the level scheme, the 279 keV transition must have an $M1$ character, resulting in the lowest state of Band 2 having a spin and parity of $7/2^-$.

States of both parities (Groups C, D, and F) have been found to feed the negative parity states of this rotational band from spin 7/2 up to 21/2 (see Fig. 2). Group C was also found to feed lower lying members of Band 1. This feature of Group C will be discussed in more detail later in the text.

3. Bands 3 and 4

A cascade of five coincident prompt γ-ray transitions assigned as Group B was reported in [7]. The link between this group and the rest of the level scheme could not be established at that time. It was suggested that the lowest state has an isomeric character. However, in the present study it was found that the decay is prompt but very fragmented. Inspection of the prompt coincident spectra generated by gating on the previously floating cascade of low-energy transitions revealed new dipole γ-ray transitions with energies of 103, 143, 147, 204, 213, 232, and 263 keV, all associated with ^{193}Bi. These transitions together with the previously identified cascade of transitions form a regular rotational band (Band 3). At first, the cascade of $M1$ transitions resembles a shears band similar to the one observed in ^{197}Bi [6], only located at lower excitation energy. However, when gating on the 143 and 147 keV transitions, respectively, a group of new γ rays located around 500 keV appears in the prompt coincident γ-ray energy spectrum. Selecting various energy gate combinations enabled us to identify five new $E2$ transitions, with energies of 438, 513, 531, 574, and 596 keV. On the basis of energy sum arguments using $\Delta I = 2$ transitions, the ordering of transitions in Band 3 was deduced. Using the sum of gates of all known $M1$ members of the band resulted in the extension of the band up to an energy of 4242 keV and a spin and parity of $(37/2^-)$. The band structure starts to be irregular above spin $33/2^-$, which may indicate that a band crossing is taking place.

Many links between Band 3 and lower-lying collective and noncollective states have been identified (see Fig. 2). One of the decay paths of Band 3 proceeds via the emission of two γ-ray transitions with energies of 284 keV and 631 keV, which serve as the connecting links between Band 3 and the newly observed Band 4 (see Fig. 2).

The links to Band 2 allowed us to unambiguously determine the spin and parity of most of the Band 3 members. We assign the $19/2^-$ state as the bandhead.

As demonstrated in Fig. 5(c), the gated spectrum involves two separate groups of lower and higher-energy γ rays, which belong neither to Band 3 nor to Group F. They form a cascade of $M1$ and $E2$ transitions characteristic of a strongly coupled rotational band. The 662 keV γ-ray transition depopulates the $I^\pi = 9/2^-$ bandhead of the new strongly coupled $h_{9/2}$ band (Band 4). In our study, this band is observed up to energy of 2.241 MeV and spin and parity of $19/2^-$. Also in this band, the decay of the lower-spin states is rather fragmented.

4. Groups D and F

Gating on the γ-ray transitions from the lower part of Band 2 in the prompt γ-γ matrix revealed many new γ-ray transitions. One part of these transitions forms a separate group of states, Group D, each connected via only one transition with Band 2. All of these states are weakly populated, making it difficult to firmly assign the multipolarity to the corresponding γ-ray transitions and hence the spin and parity of the states. Nevertheless, it was possible to perform a DCO analysis for some of the transitions in the group (see Table I), thus proving negative parity for the majority of the states.

Another group of negative parity states, Group F, is next to Band 2 in Fig. 2. Here, gating on the two γ rays, 352 and 1067 keV, appearing as doublets in the recoil-gated γ-ray energy spectrum, contributed most to building of this part of the presented level scheme. The 1067 keV transition was found to depopulate the $13/2^-$ state to the $9/2^-$ ground state. By gating on this γ ray, another relatively strong $E2$ transition with an energy of 670 keV was observed. However, no other comparably strong transitions were observed, excluding the possibility of the presence of another rotational band. Many other γ-ray transitions can be identified in the γ-ray energy spectra gated on the aforementioned γ rays (see Fig. 2).

5. High-spin isomeric states

Band 5 is built on an isomeric state with a spin and parity of $(29/2^-)$ [7]. The γ-ray spectrum observed with the focal plane Ge detectors within 15 μs after a recoil implantation in the DSSDs is shown in Fig. 6(a). The prominent peaks in this spectrum are associated with the decay of this isomeric state. The half-life of the isomeric state was remeasured with a final value of $T_{1/2} = 3.02(8)$ μs. This value was obtained by projecting and fitting the time differences between the detection of the (ΔE-ToF condition) recoil and delayed γ-ray transition with an energy of 307 keV at the focal plane, which is the most intense transition in the delayed γ-ray spectrum within the time window Δt(recoil-delayed γ) = 0–15 μs [see Fig. 6(a)]. The measured value for the half-life is consistent with that in [7].

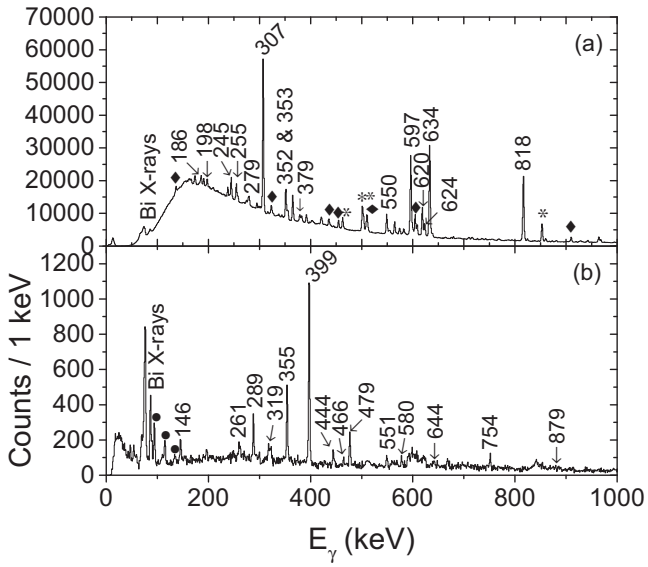

FIG. 6. (a) A spectrum of γ rays observed with the focal plane Clover detectors within 15 μs after the recoil implantation in the DSSD. Transitions marked with an energy label form the deexcitation path of the 3 μs isomer. Peaks marked with diamonds represent γ-ray transitions from the decay of the $29/2^+$ isomer (see Fig. 2) and those with asterisks belong to ^{192}Pb. (b) Prompt γ-ray spectrum gated on the 307 keV delayed γ-ray transition. Peaks marked with circles belong to ^{165}Ho.

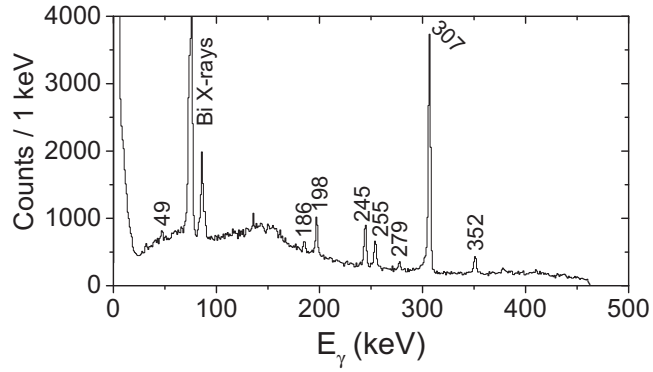

FIG. 7. An energy spectrum of γ rays detected in the planar detector in prompt coincidence with the strongest γ-ray transitions in Band 2 detected in the focal plane clover detectors within 15 μs after recoil implantation.

In order to examine the feeding pattern of the $(29/2^-)$ isomer, a γ-γ coincidence matrix of prompt transitions using the isomer-tagging technique was used. Here only those prompt γ-ray transitions which were in delayed coincidence with the transitions detected at the focal plane detectors within a specific time interval are detected. The γ-ray energy spectrum of prompt transitions in delayed coincidence with the 307 keV transition detected in the focal plane Ge detectors is shown in Fig. 6(b). Several new γ-ray transitions were found, extending the structure feeding this isomer to higher spin and energy, forming a bandlike structure Band 5 (see Fig. 2).

Since the 307 keV transition is also seen in the prompt γ-ray data, the de-excitation of this isomeric state must proceed via emission of another, low-energy γ-ray transition. As discussed in [7], the transition depopulating the isomeric state, with an upper energy limit of 60 keV and assigned $E2$ character, appears to be strongly converted. It is therefore difficult to observe in the focal plane data of this experiment, as the PIN diode detector threshold was close to 100 keV.

The γ-ray energy spectra detected in the planar detector in coincidence with individual transitions below the isomeric state do not give clear evidence for such a transition. However, the summed coincidence spectrum in Fig. 7 gated on all strong transitions in Band 2 detected in focal plane clovers shows a transition at 49 keV, which fits well within the energy limit set by the systematic studies. A peak at the same energy also appears in the planar spectrum tagged by the prompt γ-ray transitions feeding the isomer, detected in JUROGAM II. We therefore attribute the 49 keV transition to the decay of the $(29/2^-)$ isomer, which implies an excitation energy of 2.405 MeV for this state.

A conversion electron intensity analysis using the information obtained from the delayed γ-ray gated PIN spectra (γ-electron coincidences) resulted in a conversion electron intensity ratio $K/(L+M+\cdots) = 1.37(12)$ for the 307 keV transition, matching the theoretical value 1.26(4) for an $E2$ transition [41]. An $E2$ character assignment for this transition is also supported by the DCO ratio, which is 1.28(13), hence indicating a stretched quadrupole transition. Based on the intensity balance between the 49 and 307 keV transitions, we get an internal conversion coefficient of $\alpha_{\rm tot} = 185(20)$ for the 49 keV transition. This is in good agreement with the theoretical value $\alpha_{th,Tot} = 192(3)$ for an $E2$-type transition [41]. This observation makes the ^{193}Bi the lightest Bi isotope, in which the full decay path of the $29/2^-$ isomer has been observed so far. The only other known cases are ^{203,205,207}Bi [42,43], where the decay of the isomer proceeds via an $E1$ transition.

The previous study of ^{193}Bi [7] also revealed the existence of another long-lived isomer. Due to the limitations of the DAQ system, only a lower limit of $\geqslant 10$ μs for the half-life was suggested. The transitions forming part of the fragmented de-excitation path from the isomeric state are visible in Fig. 6(a). As can be seen, the statistics were poor for the relevant transitions using a search time of 15 μs. Any attempt to gain more statistics using a longer search time between recoil implantation and the detection of the delayed γ-ray transitions failed due to increasing background. To overcome this difficulty, recoil-electron correlations were employed. By selecting only those delayed transitions which were in prompt coincidence with electrons detected in the same DSSD pixel as the recoil within 15–400 μs (15 μs starting time due to electronic read-out dead-time), the spectrum presented in Fig. 8(a) was generated.

From the focal plane data, we confirmed the observations in [7], that a long-lived isomeric state de-excites via the 2110 and 2129 keV states. Using the γ-γ data from Ge detectors at the focal plane and the same isomer-tagging technique as in Fig. 8(a), many new γ-ray transitions associated with the

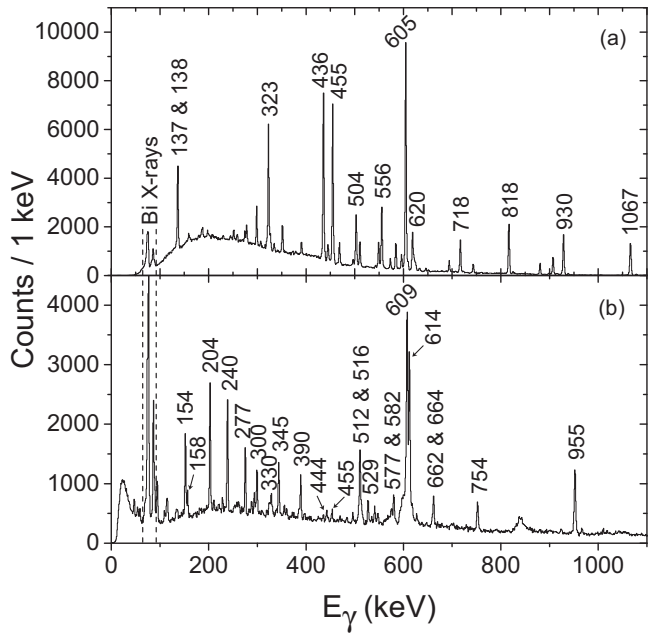

FIG. 8. (a) A spectrum of γ rays detected at the focal plane, in prompt coincidence with the electrons detected in the same DSSD pixel as a recoil within 15–400 μs. (b) An energy spectrum of prompt γ rays followed by the decay of a long-lived isomer at the focal plane [panel (a)]. The most prominent peaks are marked with an energy label.

decay of this isomeric state were identified, see Group C in Fig. 2. By applying a 15 μs – 3 ms search time window for the delayed γ-ray transitions and gating on γ-ray transitions located immediately below the isomeric state, the half-life of this isomeric state could be determined. The time-projection (recoil-γ Δt) of the 455 keV transition is shown in Fig. 9, indicating that the half-life is 85(3) μs. Similar lifetimes are obtained by selecting or combining different γ-ray transitions

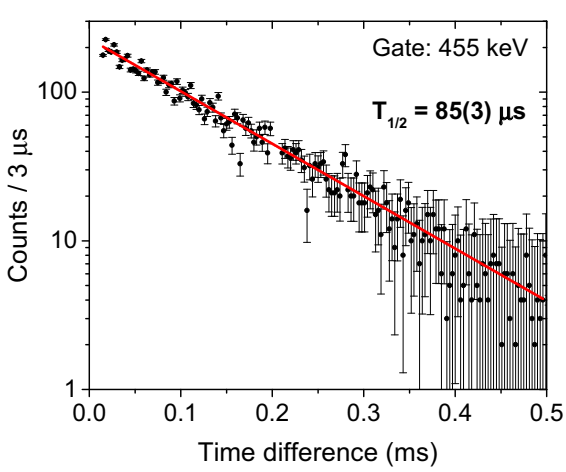

FIG. 9. (Color online) Spectrum of time differences between the observation of a recoil and of the 455 keV γ rays (from one of the many transitions below the long-lived isomer) at the RITU focal plane. An exponential decay function was fitted to the data and is shown as the solid line through data points.

depopulating the states located below the isomer, and therefore they are not shown here separately.

It is evident that one 138 keV transition is not enough to explain the γ-γ coincidences. A 138 keV transition is placed between the 1673 and 1536 keV states as in [7] and assigned to be of $M1$ character. Another 137 keV transition is placed feeding the 2129 keV state. The de-excitation path from the high-spin isomeric state proceeds via this 137 keV transition. Analysis of prompt γ-γ data from JUROGAM II gives a consistent result for Group C. The higher lying levels in Group C are based on the JUROGAM II data only. The 137 keV transition from the 2266 keV state cannot de-excite the isomeric state, because it also appears in the JUROGAM II data. In the γ-ray spectra as obtained from the planar detector at the focal plane, a transition with an energy of 84 keV is observed in coincidence with the 138, 436, and 455 keV transitions. Assuming that the 84 keV γ-ray transition depopulates the isomer, based on the energy sum arguments, the 85 μs isomer is located at an excitation energy of 2350 keV.

Another constraint for the excitation energy of the 85 μs isomeric state comes from the isomer-tagged JUROGAM II data. The prompt γ-ray energy spectrum shown in Fig. 8(b) is collected from the isomer-tagged events detected in the JUROGAM II array, applying a 15–400 μs recoil-electron correlation time gate, combined with the prompt coincidences between delayed γ rays and correlated electrons. In this spectrum, γ-ray transitions assigned to the upper part of Band 1 appear. The strong 614 keV transition, visible also in Fig. 5(a), connects the isomeric state and Band 1, as shown in Fig. 2. The cascade 158 keV + 609 keV provides a parallel path. The 609.1 and 614.0 keV γ-ray transitions and the 158 keV transition are assigned with a stretched dipole character. Provided that the scheme for Band 1 is correct, the isomeric state has a spin and parity $I^\pi = 29/2^+$ and lies at 2350 keV.

The other γ-ray transitions present in Fig. 8(b) form a structure labeled as group E. The $31/2^+$ states in Band 1 and Group E lie only $\sim$ 5 keV apart (see Fig. 2 for details). Mixing of these states most likely explains the decay path from Band 1 to the $29/2^+$ isomeric state.

The isomer-tagged data collected at the RITU focal plane were also used to extract the internal conversion coefficients for several important transitions. For this purpose, the transition intensities in Figs. 8(a) and 10 were compared. The 323 keV transition was used in order to obtain the normalization factor between these two spectra. The electron detection efficiences for PIN diode detectors have been taken from [44]. The peak with the lowest energy observed in the Re-DSSD-X-electron correlated PIN energy spectrum shown in Fig. 10 is located at $\sim$ 120 keV and corresponds mainly to L-conversion of the 137.1 and 137.6 keV transitions. Electrons originating from conversion of low-energy transitions, namely 155, 159, 186, 188, and 198 keV, contribute to this peak, but their contribution is negligible in most cases. Nevertheless, the intensity coming from the K conversion of the 198 keV $M1$ transition needed to be subtracted. The theoretical values of $\alpha_{th}(L + M + \cdots)$ for 137 keV $E2$ and 138 $M1$ transitions are 1.48(2) and 0.77(1) [41], respectively. The experimental value we obtained from the isomer-tagged PIN diode spectrum, $\alpha(L + M + \cdots) =$ 1.35(20), is well understood as a weighted average of the two

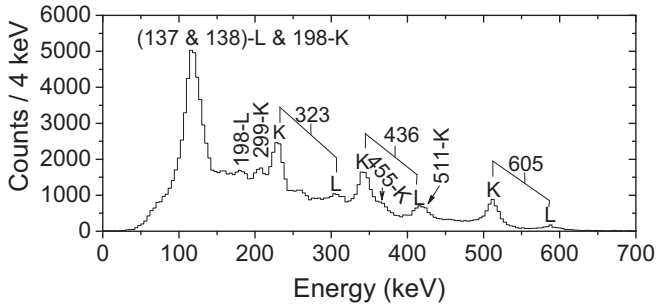

FIG. 10. Recoil-DSSD-X-electron correlated conversion-electron energy spectrum detected in PIN diodes, requiring a prompt coincidence between the DSSD-X and PIN detectors; Δt(Re-DSSD-X-e^-) = 15–400 μs. Peaks marked as L-conversion peaks also include contributions from electrons escaped from $M + N + \cdots$ shells.

theoretical values. Due to the energy threshold, L conversion of the 84 keV γ-ray transition cannot be seen in Fig. 10.

Information contained in Fig. 10 also confirms the character of the 436 and 455 keV transitions.

The intensities of the peaks corresponding to K conversion of the 436 and 455 keV transitions are very different. Since the γ-ray transition intensities of these two transitions are almost the same, they must be of different character. The extracted K-conversion coefficients are (a) 436 keV, $\alpha_K = 0.133(19)$ and (b) 455 keV, $\alpha_K = 0.032(6)$. These match rather well with the theoretical values: (a) $\alpha_{th,K} = 0.1379(20)$ for a pure $M1$ transition and (b) $\alpha_{th,K} = 0.0262(4)$ for a pure $E2$ transition [41]. By combining the experimental conversion coefficient values with the information on linear polarization factors and DCO ratios, we can conclude that the 455 and 137 keV transitions both have an $E2$ character. This yields a state with a spin and parity of $25/2^+$ at 2266 keV (see Fig. 2), depopulated by a 137 keV transition. Consequently, it implies an $E2$ character for the 84 keV transition.

The decay of the states below the isomer is rather fragmented. The number of decays to positive ($M1$ transitions) and negative parity states ($E1$ transitions) is almost equal. Examination of the prompt γ-γ data together with the analysis of the delayed part of the isomer-tagged data, enabled us to unambiguosly identify the second $13/2^+$ state (Group C) in this nucleus. It mainly decays via the emission of a 511 keV γ ray to the $13/2^+_1$ state. The possibility of having an $E0$ component was excluded based on the transition intensity analysis, and the transition was assigned a mixed $M1 + E2$ character. Another main decay branch of the $13/2^+_2$ state is to the $11/2^-$ member of Band 2, via a 497 keV $E1$ transition.

6. Band 6

The $1/2^+$ proton intruder state located at 307(7) keV [37] predominantly decays via the emission of an α particle. The structure feeding the intruder state can therefore be studied by means of the RDT method, where, by gating with the recoil decay events (in this work α particles), one can select the transitions in prompt coincidence with the preceding recoil. The level sequence above the $1/2^+$ intruder state was reported

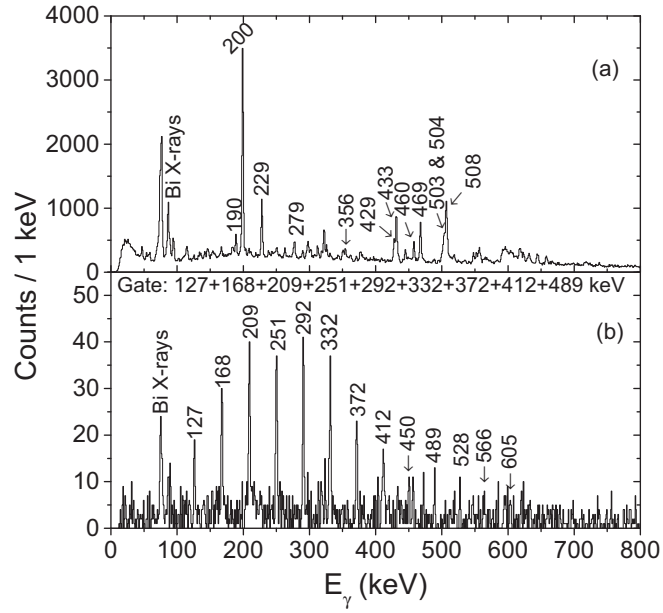

FIG. 11. (a) Singles spectrum of γ rays tagged by the α decay of the $1/2^+$ proton intruder state and using a search time of 9.6 s. (b) Sum of prompt γ-ray spectra gated with transitions in the superdeformed band assigned to ^{193}Bi. A matrix of γ-γ coincidences between JUROGAM II detectors tagged with the α decay of the $1/2^+$ intruder state was used.

for the first time in [7], with only a tentative spin assignment. The 200 keV transition, tentatively assigned with $M1$ character was placed directly feeding the $1/2^+$ state. The location of several transitions remained unresolved. In the present work, analysis of α-tagged data allowed a regular band-like structure to be constructed feeding the $1/2^+$ intruder state. In this study, the uppermost state of the band has a spin and parity $I^\pi = (17/2^+)$ and energy 2.141 MeV. In Fig. 11(a) the newly observed transitions can be seen in the prompt γ-ray spectrum tagged with the 6475 keV α particles from the decay of the $1/2^+$ state.

Different half-lives for the $1/2^+$ state can be found in the literature, e.g. namely $T_{1/2} = 1.9(4)$ s [37], $T_{1/2} = 3.15$ s [45] and $T_{1/2} = 3.48(18)$ s [46]. In our study, a search time of 9.6 s was used. Decay time analysis using the logarithmic time scale method [47] of the α-tagged data was performed. In the present experiment, the random rate in the DSSDs was comparable to the half-life of the $1/2^+$ state. The unwanted background in the decay-time distribution originates mainly from random and α-particle-like treated recoils and scattered beam (no energy signal in the MWPC). To reduce its effect, only three corners of the DSSD (10 × 10 strips size) were used to collect the necessary information from the part of data recorded at a lower count rate. The distribution obtained by this method (by Eq. 8 in [47]) together with corresponding fit is presented in Fig. 12. This fit gives an apparent half-life 2.68(4) s for the $1/2^+$ intruder state. The random background peak with its half-life of 21(1) s is not well separated from the $1/2^+$ state decay-time peak as displayed in Fig. 12.

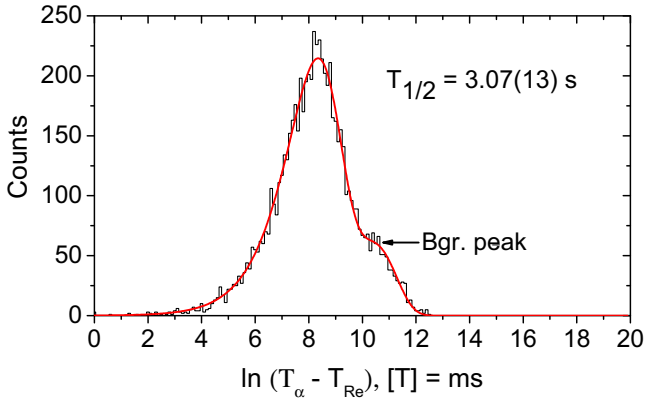

FIG. 12. (Color online) The distribution of time differences between the recoil implantation T_{Re} and the detection of a subsequent α particle T_α from the α decay of the $1/2^+$ state in three corners of the DSSD. Only part of data with lower count rate of recoils was used to generate this distribution. The distribution was fitted using the two-component fit (the solid curve through data points). The displayed half-life is corrected for the background contribution.

An additional correction [48] to the half-lives obtained by applying the method described in [47] must be made, when the half-life is not much shorter than the value of related random recoil rate. The distribution obtained with $T_{1/2} = 2.68$ s in Fig. 12 involves also some events, where the α decay is correlated with a random recoil. Therefore, the fitted decay constant is sum of $\lambda_{1/2^+}$ and $\lambda_{bgr.}$. The final half-life deduced from the decay-time distribution with lower recoil counting rate and corrected for the contribution from the random background has a value of 3.07(13) s.

The $7/2^-$ bandhead of Band 2 located at 279 keV makes it possible for the $1/2^+$ state to also decay via an electromagnetic transition. The resulting 28(7) keV transition would be of E3 character, and hence highly converted. However, correlation with electrons did not provide a clean spectrum in this case and its efficiency was rather low.

B. Superdeformed band

The analysis of the data revealed the presence of a band of thirteen coincident transitions extending from 127 to (605) keV (see Fig. 11(b) and Table II) with an average energy difference of 40 keV, i.e., consistent with the spacing expected for a superdeformed (SD) shape in this region [21]. This SD band was found by tagging on α decays of the $1/2^+$ proton intruder state, and represents $\sim 3.9\%$ of the total population of this state. The spectrum presented in Fig. 11(b) is the sum of spectra in coincidence with the cleanest gates. The cascade character of these transitions was confirmed by summing the spectra gated on all transitions from 127 to 412 keV, plus 489 keV in LEVIT8R [35,36] using the recoil-gated γ-γ-γ cube. No signature partner of this band was found.

Gamma-ray transitions related to the decay of the SD band to the $1/2^+$ intruder band were searched for energies up to 4 MeV. If the bandhead of SD band would decay via one transition to the 307 keV level, this should be clearly observed. There is evidence of a weak γ-ray transition with an energy of about 1836 keV in the α-tagged data, which is in clear coincidence with some transitions of the observed SD band in ^{193}Bi (see Fig. 13). More statistics is required to confirm the possible linking transition connecting the SD band and Band 6.

TABLE II. The energy (E_γ), relative intensity ($I_{\gamma(\alpha)}$) in the α-tagged gated spectrum, relative intensity ($I_{\gamma(\text{rec.})}$) in the recoil-gated spectrum (Re-γ-γ-γ), excitation energy (E_i), and spin and parity (I_i^π and I_f^π) of the initial and final states of the γ-ray transitions assigned to the SD band in ^{193}Bi. The statistical error of about 0.3 keV should be added to the fitting errors given for most of the transitions listed in the first column.

E_γ (keV)	$I_{\gamma(\alpha)}$ (%)	$I_{\gamma(\text{rec.})}$ (%)	E_i (keV)	I_i^π	I_f^π
126.6(2)[a]	0.7(2)		X + 127	$(15/2^+)$	$(11/2^+)$
168.3(1)	1.5(3)	0.8(6)	X + 295	$(19/2^+)$	$(15/2^+)$
209.5(1)	2.0(2)	1.2(3)	X + 504	$(23/2^+)$	$(19/2^+)$
250.9(1)	1.9(4)	2.0(4)	X + 755	$(27/2^+)$	$(23/2^+)$
291.7(1)	1.8(4)	1.8(3)	X + 1047	$(31/2^+)$	$(27/2^+)$
331.7(1)	1.6(4)	2.3(3)	X + 1379	$(35/2^+)$	$(31/2^+)$
372.2(1)	1.1(3)	1.7(2)	X + 1751	$(39/2^+)$	$(35/2^+)$
411.8(1)	0.8(2)	1.3(2)	X + 2163	$(43/2^+)$	$(39/2^+)$
450.4(2)	0.4(1)	1.3(2)	X + 2613	$(47/2^+)$	$(43/2^+)$
489.2(2)	0.4(1)	0.9(2)	X + 3102	$(51/2^+)$	$(47/2^+)$
527.8(1)	0.3(1)	1.4(2)	X + 3630	$(55/2^+)$	$(51/2^+)$
(566.0(2))	0.2(1)	1.1(2)	X + (4196)	$(59/2^+)$	$(55/2^+)$
(604.5(1))	0.2(1)	2.0(3)	X + (4800)	$(63/2^+)$	$(59/2^+)$
1836(5)[b]	0.9(2)				

[a] $I_{\gamma(\text{rec.})}$ could not be obtained from the LEVIT8R.
[b] A γ-ray transition seen in mutual coincidence with 168.3 and 331.7 keV transitions.

IV. DISCUSSION

The nucleus ^{193}Bi lies in a transitional region, since in the lighter Bi isotopes deformed structures dominate, whereas in the heavier isotopes the yrast structures can be explained assuming a spherical shape. We present the experimental data exhibiting an extensive manifestation of shape coexistence, as

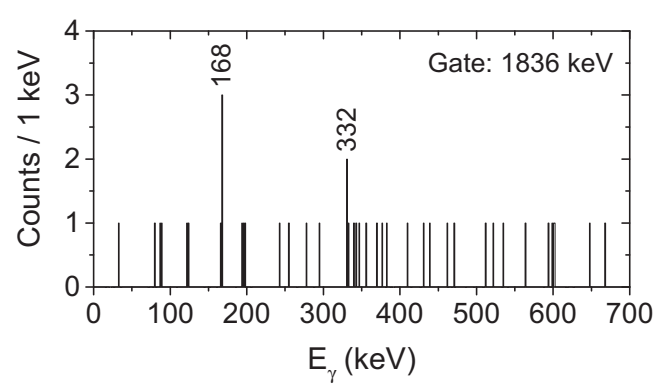

FIG. 13. An energy spectrum of prompt γ rays tagged by the α decay of the $1/2^+$ proton intruder state and in coincidence with the 1836 keV transition.

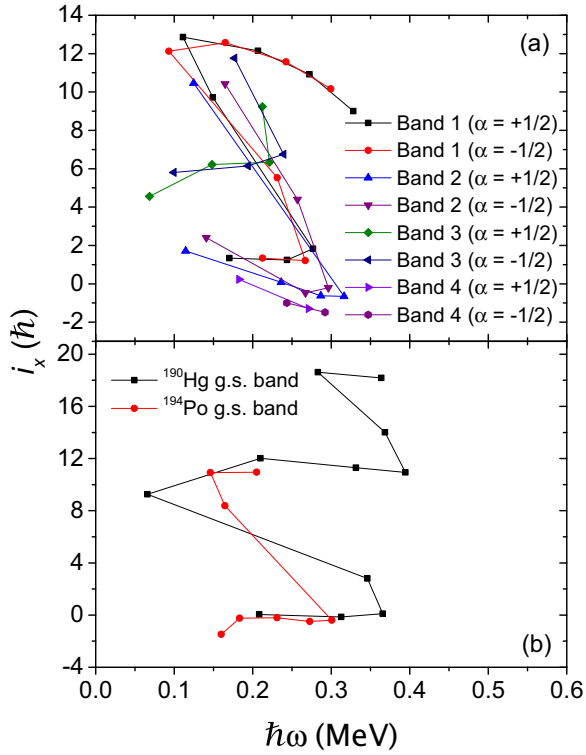

FIG. 14. (Color online) Aligned angular momenta i_x for the (a) favored ($\alpha = +1/2$) and unfavored ($\alpha = -1/2$) signatures of Band 1 ($\pi 13/2^+[606]$), Band 2 ($\pi 7/2^-[514]$), Band 3 ($\pi i_{13/2} \otimes \nu i_{13/2} p_{3/2}$, $K = 9.5$) and Band 4 ($\pi 9/2^-[505]$) in ^{193}Bi. (b) Yrast bands in ^{190}Hg [51] and ^{194}Po [52]. In case of the Bi and Po isotopes, a reference with the Harris parameters $J_0 = 13\ \hbar^2$/MeV and $J_1 = 219\ \hbar^4$/MeV^3 has been subtracted. Harris parameters $J_0 = 3\ \hbar^2$/MeV and $J_1 = 85\ \hbar^4$/MeV^3 have been used for the rotational reference in ^{190}Hg.

both collective oblate and spherical structures can be expected in ^{193}Bi. Such an admixture of structures is most likely the explanation for the richness of the level structures observed in ^{193}Bi. In the following several observed level structures will be discussed. To facilitate the discussion of rotational bands, aligned angular momenta and $B(M1)/B(E2)$ ratios are shown in Figs. 14 and 15. Theoretical estimates for the $B(M1)/B(E2)$ ratios have been calculated using the semiclassical formalism of Dönau and Frauendorf [49,50]. Most of these bands can be described by the coupling of an unpaired proton to the semimagic lead core.

A. Normally deformed states

1. Band 1: $i_{13/2}$

The isomeric $13/2^+$ state in the neutron-deficient bismuth isotopes can be understood as the coupling of an $i_{13/2}$ proton to the oblate 2p-2h 0^+ intruder state of the ^{192}Pb core. The smoothly increasing behavior of the transition energies of the resulting strongly coupled band built on top of this isomeric state terminates when the $25/2^+$ state is passed. In Fig. 14(a), the aligned angular momentum i_x as a function of the rotational frequency for Band 1 is presented. A sharp band crossing takes place at $\hbar\omega \sim 0.2$ MeV, with about 10–11 $\hbar$ gain in alignment. For comparison, alignment plots for the ground state bands in ^{190}Hg and ^{194}Po are shown in Fig. 14(b). The total gain in alignment in Band 1 and the crossing frequency are consistent with those for ^{190}Hg and ^{194}Po. In these two even-even nuclei, the alignments have been attributed to the two $i_{13/2}$ neutrons, which is most likely the case also for Band 1. Sharp $i_{13/2}$ neutron alignments appear to be typical in this mass region for low and moderate oblate deformations. The $B(M1)/B(E2)$ ratios for Band 1 are shown in Fig. 15(a). Theoretical calculations using parameters taken from [7] nicely follow the experimental pattern, both below and above the band crossing.

2. Bands 2 and 4

Band 2 is built on the 7/2[514] Nilsson configuration (mixed $h_{9/2}/f_{7/2}$). As can be seen in Fig. 14(a) the same trend in the evolution of i_x as a function of rotational frequency is observed as in the case of Band 1. Here, the smooth increase of the $E_\gamma(E2)$ ends at $I^\pi = 23/2^-$. In our data, Band 2 has been extended up to spin $29/2^-$ only, which seems to be the point with the maximum gain in the alignment brought by the $i_{13/2}$ neutron pair in this rotational band. After the neutron $i_{13/2}$ alignment, Band 2 is expected to be as yrast as Band 1. Unexpectedly, for some reason the band was not seen beyond the band crossing in the experiment. The theoretical $B(M1)/B(E2)$ ratios follow the experimental values [see Fig. 15(b)].

Band 4 seems to be quite regular and similar to Band 2. The extracted aligned angular momenta for Band 4 shown in Fig. 14(a) are slightly lower than those in Band 2. We assign the 9/2[505] configuration to this band. Theoretical estimates for the proposed configuration reproduce the experimental $B(M1)/B(E2)$ ratios in Fig. 15(d) when a somewhat lower quadrupole moment is assumed compared to other bands in ^{193}Bi.

3. Band 3

Based on the bandhead energy of Band 3 and assigned spin values, it is most likely built on a three-quasiparticle (qp) configuration. From the aligned angular momentum plot shown in Fig. 14(a) one can see that the gain of about 6–7 $\hbar$ in alignment with maximum possible $K = 9.5$ chosen ($I_{b.h.} = 19/2^-$) can be observed. Such an aligned angular momentum suggests one $i_{13/2}$ neutron in the configuration. Since negative parity was assigned for Band 3, a configuration with an $i_{13/2}$ proton and neutron coupled to a neutron occupying one of the negative parity orbitals close to Fermi surface is proposed. The 7^- and 9^- states in Po isotopes and their Pb isotones have been assigned with almost pure neutron 2 qp configurations, $\nu(i_{13/2}^{-1} p_{3/2}^{-1})$ and $\nu(i_{13/2}^{-1} f_{5/2}^{-1})$ for 7^- and 9^-, respectively [52]. If we assume the same oblate deformation here as for Band 1, the calculated $B(M1)/B(E2)$ ratios reproduce the experimental values, especially at higher spin [see Fig. 15(c)]. This is a remarkably good agreement, since Band 3 involves three quasiparticles in its configuration.

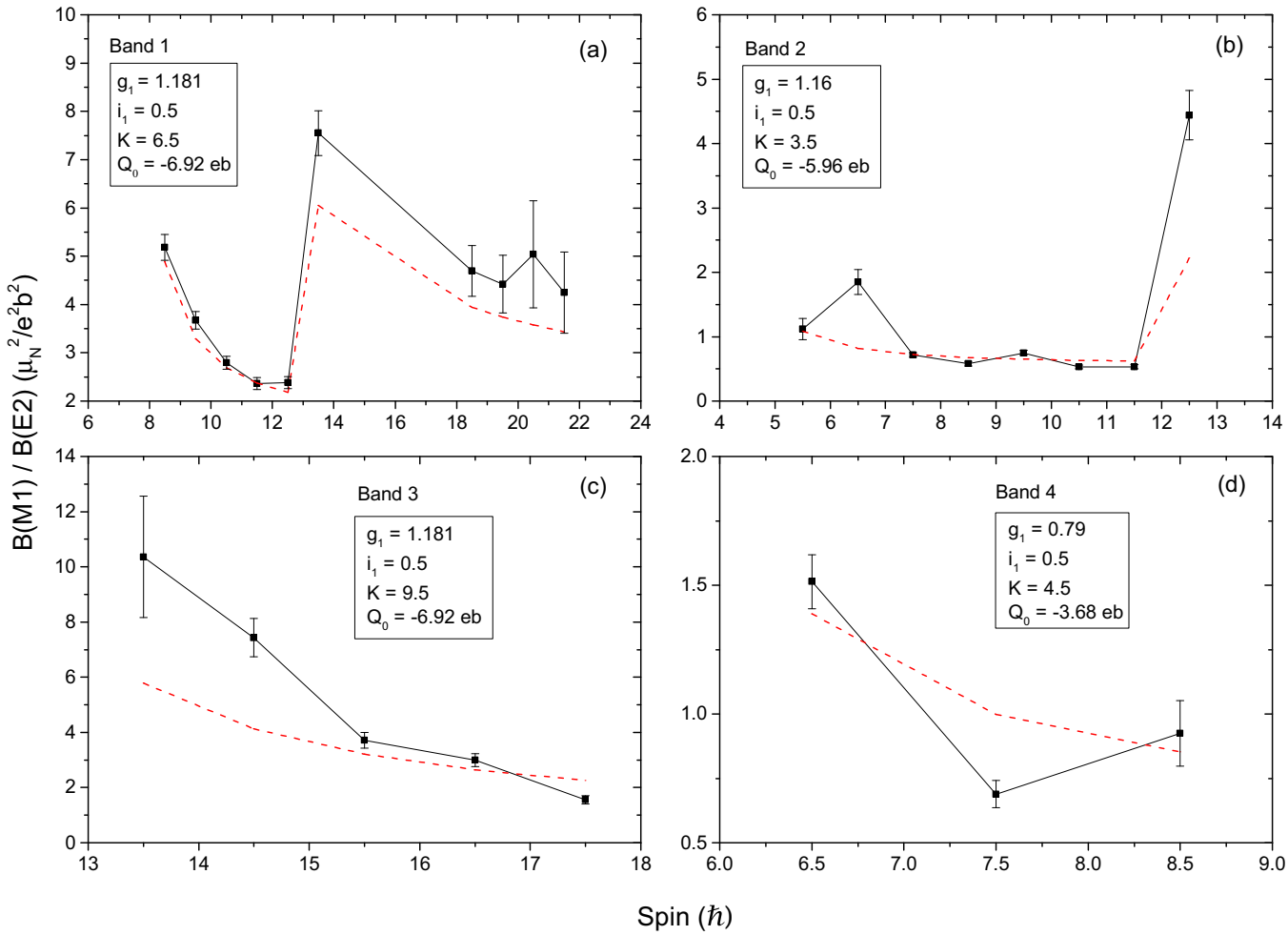

FIG. 15. (Color online) Experimental $B(M1)/B(E2)$ ratios for (a) Band 1, (b) Band 2, (c) Band 3, and (d) Band 4 in ^{193}Bi together with semi-empirical estimates. The parameter values for the odd proton used in the calculations are indicated.

4. Band 5

Most of the high-spin states in heavier odd-A Bi isotopes can be explained by the coupling of an $h_{9/2}$ proton to the Pb core states [9,43,53,54]. Based on systematics, the $29/2^-$ states can be associated with the $\pi h_{9/2} \otimes \nu(i_{13/2}^{-2})_{12^+}$ multiplet [5]. The $29/2^-$ state together with the $31/2^-$ and $33/2^-$ states are interpreted to be of the same configuration. The $29/2^-$ state keeps its isomeric character throughout the Bi isotopic chain up to ^{207}Bi, where its energy is about 1.5 MeV higher, whereas the half-life drops down to 12.7(9) ns [43] from 3 μs in ^{193}Bi. The $\pi h_{9/2} \otimes \nu(i_{13/2}^{-2})_{10^+}$ configuration is assigned for the $25/2^-$ state populated by the 49 keV transition. The reduced transition strength for this transition is 0.052(2) W.u. It seems to be slightly hindered when compared to 0.160 and 0.466 W.u. for the corresponding $12^+ \rightarrow 10^+$ core transitions in ^{192}Pb [55] and ^{194}Pb [56], respectively.

We note that Band 5 has the same quasiparticle configuration as Band 2 after the neutron $i_{13/2}$ alignment. While spherical shape is assumed for at least the few lowest members of Band 5, oblate shape is attributed to Band 2. However, Band 5 has a rotational-like character at higher spins. It is possible that the shape changes towards oblate shape in Band 5 at higher spin. It remains to be seen in future experiments whether there are connections from the uppermost members of Band 5 to Band 2.

5. Band 6

The irregular bandlike structure (Band 6) is built on the $1/2^+$ proton intruder state, which is of 2p-1h nature. The hole state determining the spin and parity of this intruder state is created by exciting and coupling a proton from $3s_{1/2}$ 1/2[400] Nilsson orbital to an odd-proton in the $1h_{9/2}$ 9/2[505] Nilsson orbital. An oblate shape is attributed to such a configuration in odd-mass Bi nuclei [7].

Small increases in alignment at low spin for ^{191,193}Bi in Fig. 16 can be observed. Nyman *et al.* [8] attribute this gain in the alignment in ^{191}Bi to the crossing of a level structure with a lower deformation by a more deformed structure. We can speculate that in ^{193}Bi a similar shape change occurs, but at a slightly higher rotational frequency.

Corresponding states have been recently observed also in ^{199,201}At [57] (see the level systematics therein for more details).

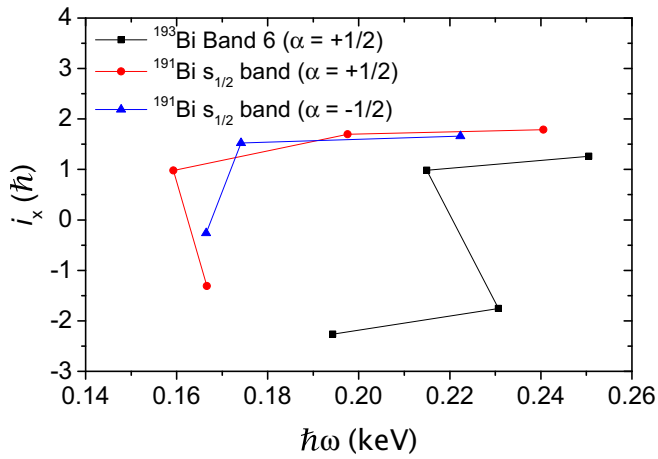

FIG. 16. (Color online) Aligned angular momenta i_x for Band 6 in ^{193}Bi and the $s_{1/2}$ band in ^{191}Bi. A reference with the Harris parameters $J_0 = 13\ \hbar^2$/MeV and $J_1 = 219\ \hbar^4/\text{MeV}^3$ has been subtracted.

B. High-spin isomer $29/2^+$

Owing to the excitation energy, the $29/2^+$ isomeric state has also a 3 qp configuration. High-spin states in odd-A Bi isotopes were under intense investigation in the late 1970s and early 1980s, mainly studies carried out by Lönnroth *et al.* [9,43,53,54] and Hübel *et al* [4,42], but no corresponding isomeric states have been reported. As shown in Fig. 17, in heavier odd-A Bi isotopes the yrast $21/2^+$ and $25/2^+$ states are well known and these states were found to remain isomeric up to ^{207}Bi [43,53,58]. These isomeric states were previously

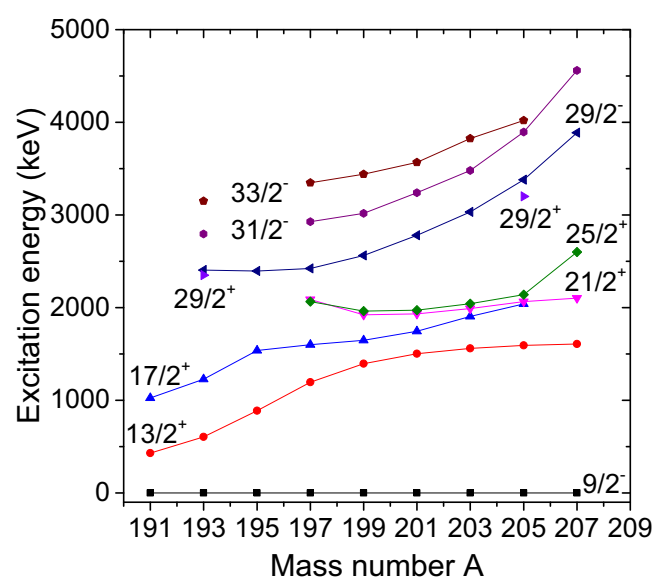

FIG. 17. (Color online) Systematics of selected excited states in odd-A Bi isotopes. Where the exact excitation energy is not known due to unobserved low-energy transitions Δ, it is set to 40 keV for clarity. The data are taken from [9,10] (^{195}Bi), [6,59] (^{197}Bi), [5] (^{199}Bi), [5,60] (^{201}Bi), [4,42,54] (^{203}Bi), [42,54,61] (^{205}Bi), [43,53,58] (^{207}Bi), and for ^{193}Bi from the present work.

explained as a $\pi h_{9/2}$ coupled to 7^- and 9^- states in Pb isotones [5]. Configurations associated with these states cannot give rise to an isomeric state with spin 29/2.

In the odd-A At isotopes, $29/2^+$ isomeric states have been observed [11–15]. They are assigned to the $\pi(i_{13/2}h^2_{9/2})$ configuration. Jakobsson *et al.* [14] reason that the major difference between the two configurations, that of the $29/2^+$ state and the states due to coupling of the odd $h_{9/2}$ proton to the negative parity states below the 11^- isomer in the Po core results in the $29/2^+$ state becoming isomeric. We propose the same configuration for the $29/2^+$ isomeric state in ^{193}Bi. In contrast with the At isotopes, such a configuration in Bi requires the excitation of a proton pair across the $Z = 82$ shell gap. This might well explain the higher excitation energy of this state in Bi, even though no such state has yet been observed in the At isotone. In ^{201}At a reduced transition strength $1.26(4) \times 10^{-3}$ W.u. [62] has been deduced for an $E2$ transition depopulating the $29/2^+$ isomer. The experimentally observed 84 keV $E2$ transition depopulating the $29/2^+$ state in ^{193}Bi has a reduced transition strength $1.6(1) \times 10^{-3}$ W.u.. This perfectly matches with the value of reduced transition strength 1.6×10^{-3} W.u. for the corresponding $E2$ transition for the $11^- \rightarrow 9^-$ isomeric decay in ^{194}Pb [56]. The reduced transition strengths for the corresponding $E2$ transitions in ^{192}Pb [55] and ^{196}Pb [63] are 1.42×10^{-2} W.u. and 21×10^{-5} W.u., respectively. A similar increasing trend of $B(E2)$ values as in Pb isotopes has also been observed for At isotopes (see, e.g., Ref. [15] and references therein) and one can speculate that $B(E2)$ values rather similar to those in ^{193}Bi and ^{194}Pb will also be observed in ^{197}At.

The most likely scenario here is that the $29/2^+$ state is a result of coupling of the $i_{13/2}$ proton to the oblate $8^+[\pi h^2_{9/2}]$ state in ^{192}Pb. This is in agreement with the configuration proposed by Nieminen *et al.* [7] for an isomeric weakly oblate band with $K = 29/2$, even though there the coupling of the $h_{9/2}$ proton to Pb_{11^-} core state was suggested.

The $31/2^+$, $33/2^+$, $35/2^+$, and $37/2^+$ states at 2959, 3304, 3886, and 4272 keV, respectively, are interpreted as members of the band on top of the $29/2^+$ state. The negative parity states in Group E may arise from coupling of the $29/2^+$ state to the 7^- and 9^- states ($\nu i_{13/2}p_{3/2}$ and $\nu i_{13/2}f_{5/2}$ configurations) in even-even neighbors [52,64].

The de-excitation path from Band 1 is rather surprising. The $31/2^+$ state in the level structure built on the isomeric state is only 5 keV apart from the $31/2^+$ state in Band 1. These two states apparently mix, where from the intensities of the 154 and 158 keV transitions one can estimate the amount of mixing assuming a simple two-state mixing model. The basic wave functions of the two $31/2^+$ states are products of the $\pi i_{13/2} \otimes \nu i^2_{13/2}$ (oblate) and $\pi i_{13/2}h^2_{9/2}$ (oblate) configurations. The mixing amplitudes deduced from the experimental ratio of $B(M1)$ probabilities are $\alpha = 0.96$ and $\beta = 0.27$. This implies an interaction energy of 1.3 keV and corresponds to an energy shift of $0.085\Delta E_u$ between the perturbed and unperturbed $31/2^+$ level energies, where the ΔE_u denotes the unperturbed splitting. Such an interaction energy is consistent with that observed in ^{163}Er between rotational bands built on different three qp configurations [65]. Finally, the assumption of experimentally observed 5 keV perturbed splitting results

in $\Delta E_u = 4.27$ keV, indicating a very weak mixing of the above-mentioned configurations.

C. Noncollective states

Several positive parity states, belonging to Group C (see Fig. 2), can be interpreted by the coupling of the odd proton in the $h_{9/2}$ orbital to spherical negative parity states in ^{192}Pb. From the theoretical point of view, this has been done by using the cluster interaction approach [5,59]. Systematics of these states are shown in Fig. 17. Remarkable agreement for the $17/2^+$, $21/2^+$, and $25/2^+$ states should be emphasized. The second $13/2^+$ state can be explained as a proton occupying the spherical $i_{13/2}$ orbital. The $13/2^-$ state located at 1067 keV is attributed to the coupling of an $\pi h_{9/2}$ to a spherical 2^+ state in ^{192}Pb. Many other noncollective states in ^{193}Bi cannot be easily explained.

D. Superdeformation

Theoretical calculations predict the $\pi i_{11/2}$ $1/2^+[651]$ orbital to be the lowest configuration in the SD minimum for odd-A Bi isotopes [22,66]. The SD band observed in the present study is assigned with the favored signature of this configuration. In contrast to ^{193}Bi, in ^{191}Bi also the unfavored signature partner was found [8]. The observed band is almost identical to the more strongly populated SD band (SD1, $\alpha = -1/2$) in ^{191}Bi. The transition energies are 0–2 keV higher in ^{193}Bi. There is also a striking agreement between the SD band in ^{193}Bi and the SD band 4 in ^{193}Tl, interpreted as the negative signature of the [651]1/2 proton orbital [67]. At lower rotational frequencies, the transition energy differences are below 1 keV. Absolute transition probabilities are necessary in order to confirm the SD character of this band.

The SD minimum is calculated to lie at a lower energy in this mass region than elsewhere. According to calculations performed by Hilaire and Girod [68], in Bi nuclei a more pronounced SD minimum located at 2 MeV starts to appear in ^{188}Bi and continues to evolve in heavier isotopes. In the ^{193}Bi, such a secondary minimum should be located at ~ 2.4 MeV. In the α-tagged spectrum [see Fig. 11(b)], no transitions of Band 6 are present. This could mean that the intensity remains in the SD band down to low spins. In the observed SD band built on the $1/2^+[651]$ configuration the two lowest transitions, which are expected to have energies of about 87 and 46 keV, were not observed. On the other hand, the 87 keV transition would be overlapping with a Bi x-ray peak located at 87.4 keV in the energy spectrum. Moreover, the conversion coefficients for 46 and 87 keV $E2$ transitions are large, $\alpha_{\rm tot} = 261(4)$ and $\alpha_{\rm tot} = 12.82(18)$ [41]), respectively, making these γ-ray transitions almost impossible to observe in the α-tagged energy spectrum (shown in Fig. 12). We assume that the intensity flows via these transitions to the $3/2^+$ bandhead. Either the $3/2^+$ or the $1/2^+$ state is the lowest state for the proposed configuration.

The SD band is seen in both α-tagged γ-γ and recoil-gated γ-γ-γ data. The γ-ray intensity patterns are different for α-tagged and recoil-gated sum spectra, respectively (see Fig. 18), indicating that the SD band also feeds other states than those culminating in the $1/2^+$ isomeric state. Possible corresponding transitions could not be seen, as the RDT method providing clean γ-ray spectra cannot be employed for the $9/2^-$ ground state due to its long half-life of 67 s.

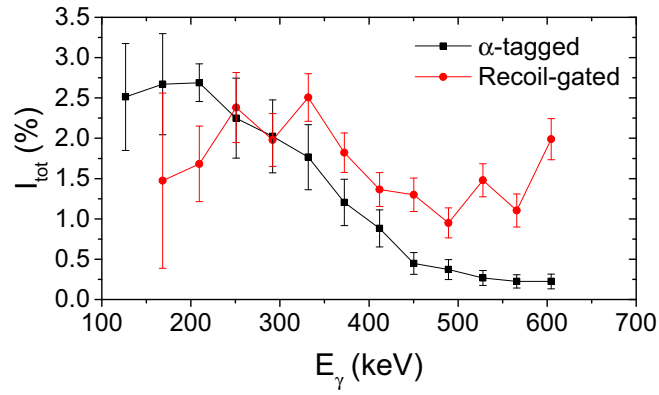

FIG. 18. (Color online) Relative transition intensity of the γ rays in the SD band of ^{193}Bi as obtained from (black) the α-tagged coincidence γ-γ matrix gated on the sum of transitions (see Fig. 13) and (red) recoil-gated γ-γ-γ cube. The data are normalized to the yield of the 323.4 keV transition.

V. CONCLUSION

In summary, excited states in ^{193}Bi have been observed using various tagging techniques. The previously known level structures were extended and new structures were revealed. Several structures can be understood assuming an oblate deformation, while some others require a spherical shape. Also, a rotational band showing properties typical for SD bands was identified. A candidate for a transition connecting the SD band with the $1/2^+$ proton intruder state was proposed. Using the GREAT spectrometer, a new long-lived isomeric state having $I^\pi = 29/2^+$ was found. We associate this state with the $\pi(h^2_{9/2} i_{13/2})$ configuration. This isomeric state de-excites via a hindered 84 keV $E2$ transition to the $25/2^+$ state of $\pi h_{9/2} \otimes \nu(i_{13/2} f_{5/2})$ parentage. In this work, the excitation energy of another isomeric state with $I^\pi = 29/2^-$ could be determined. This state is associated with the $\pi h_{9/2} \otimes \nu(i^2_{13/2})_{12^+}$ configuration.

ACKNOWLEDGMENTS

This work was supported by the Academy of Finland under the Finnish Center of Excellence Programme. The authors would like to thank the GAMMAPOOL European Spectroscopy Resource for the loan of germanium detectors for JUROGAM II.

[1] K. Heyde *et al.*, Phys. Rep. **102**, 291 (1981).
[2] R. Julin, K. Helariutta, and M. Muikku, J. Phys. G **27**, R109 (2001).
[3] A. Hürstel *et al.*, Eur. Phys. J. A **15**, 329 (2002).
[4] H. Hübel *et al.*, Nucl. Phys. A **294**, 177 (1978).
[5] W. F. Piel, T. Chapuran, K. Dybdal, D. B. Fossan, T. Lonnroth, D. Horn, and E. K. Warburton, Phys. Rev. C **31**, 2087 (1985).
[6] G. K. Mabala *et al.*, Eur. Phys. J. A **25**, 49 (2005).
[7] P. Nieminen *et al.*, Phys. Rev. C **69**, 064326 (2004).
[8] M. Nyman *et al.*, Eur. Phys. J. A **51**, 31 (2015).
[9] T. Lönnroth *et al.*, Phys. Rev. C **33**, 1641 (1986).
[10] H. Pai *et al.*, Phys. Rev. C **85**, 064317 (2012).
[11] I. Bergström *et al.*, Phys. Scr. **1**, 243 (1970).
[12] T. P. Sjoreen *et al.*, Phys. Rev. C **14**, 1023 (1976).
[13] R. F. Davie *et al.*, Nucl. Phys. A **430**, 454 (1984).
[14] U. Jakobsson *et al.*, Phys. Rev. C **82**, 044302 (2010).
[15] K. Auranen *et al.*, Phys. Rev. C **91**, 024324 (2015).
[16] E. A. Henry *et al.*, Z. Phys. A **338**, 469 (1991).
[17] S. Pilotte *et al.*, Phys. Rev. C **49**, 718 (1994).
[18] R. M. Clark *et al.*, Phys. Rev. C **53**, 117 (1996).
[19] A. N. Wilson *et al.*, Phys. Rev. Lett. **90**, 142501 (2003).
[20] A. N. Wilson *et al.*, Eur. Phys. J. A **24**, 179 (2005).
[21] R. R. Chasman *et al.*, Phys. Rev. Lett. B **219**, 227 (1989).
[22] W. Satula, S. Cwiok, W. Nazarewicz, R. Wyss, and A. Johnson, Nucl. Phys. A **529**, 289 (1991).
[23] S. J. Krieger, P. Bonche, and M. S. Weiss, Nucl. Phys. A **542**, 43 (1992).
[24] G. Duchene *et al.*, Nucl. Instrum. Methods Phys. Res., Sect. A **432**, 90 (1999).
[25] C. W. Beausang *et al.*, Nucl. Instrum. Methods Phys. Res., Sect. A **313**, 37 (1992).
[26] C. Rossi Alvarez, Nucl. Phys. News **3**, 10 (1993).
[27] A. Georgiev and W. Gast, IEEE Trans. Nucl. Sci. **40**, 770 (1993).
[28] M. E. Leino *et al.*, Nucl. Instrum. Methods. Phys. Res. B **99**, 653 (1995).
[29] J. Sarén *et al.*, Nucl. Instrum. Methods Phys. Res., Sect. A **654**, 508 (2011).
[30] R. D. Page *et al.*, Nucl. Instrum. Methods Phys. Res., Sect. B **204**, 634 (2003).
[31] I. H. Lazarus *et al.*, IEEE Trans. Nucl. Sci. **48**, 567 (2001).
[32] K. H. Schmidt *et al.*, Phys. Lett. B **168**, 39 (1986).
[33] C. Scholey *et al.*, Phys. Rev. C **63**, 034321 (2001).
[34] P. Rahkila, Nucl. Instrum. Methods Phys. Res., Sect. A **595**, 637 (2008).
[35] D. C. Radford, Nucl. Instrum. Methods Phys. Res. A **361**, 297 (1995).
[36] D. C. Radford, Nucl. Instrum. Methods Phys. Res. A **361**, 306 (1995).
[37] E. Coenen *et al.*, Phys. Rev. Lett. **54**, 1783 (1985).
[38] K. S. Krane, R. M. Steffen, and R. M. Wheeler, Nucl. Data Tables **11**, 351 (1973).
[39] K. Starosta *et al.*, Nucl. Instrum. Methods Phys. Res., Sect. A **423**, 16 (1999).
[40] O. Klein and Y. Nishina, Z. Phys. **52**, 853 (1929).
[41] T. Kibedi *et al.*, Nucl. Instrum. Methods Phys. Res. A **589**, 202 (2008).
[42] H. Hübel *et al.*, Z. Phys. A **314**, 89 (1983).
[43] T. Lönnroth, J. Blomqvist, I. Bergström, and B. Fant, Phys. Scr. **19**, 233 (1979).
[44] A. N. Andreyev *et al.*, Nucl. Instrum. Methods Phys. Res., Sect. A **533**, 422 (2004).
[45] N. I. Tarantin, A. P. Kabachenko, and A. V. Dem'yanov, Yad. Fiz. **12**, 455 (1970) [Sov. J. Nucl. Phys. **12**, 248 (1971)].
[46] H. Gauvin *et al.*, Phys. Rev. Lett. **29**, 958 (1972).
[47] K. H. Schmidt, Eur. Phys. J. A **8**, 141 (2000).
[48] M. E. Leino, S. Yashita, and A. Ghiorso, Phys. Rev. C **24**, 2370 (1981).
[49] S. Frauendorf, Phys. Lett. B **100**, 219 (1981).
[50] F. Dönau, Nucl. Phys. A **471**, 469 (1987).
[51] I. G. Bearden *et al.*, Nucl. Phys. A **576**, 441 (1994).
[52] K. Helariutta *et al.*, Eur. Phys. J. A **6**, 289 (1999).
[53] T. Lönnroth and B. Fant, Phys. Scr. **18**, 172 (1978).
[54] T. Lönnroth, Z. Phys. A **307**, 175 (1982).
[55] A. J. M. Plompen *et al.*, Nucl. Phys. A **562**, 61 (1993).
[56] M. Kaci *et al.*, Nucl. Phys. A **697**, 3 (2002).
[57] K. Auranen *et al.*, Phys. Rev. C **90**, 024310 (2014).
[58] I. Bergström *et al.*, Phys. Rev. **181**, 1642 (1969).
[59] T. Chapuran, K. Dybdal, D. B. Fossan, T. Lonnroth, W. F. Piel, D. Horn, and E. K. Warburton, Phys. Rev. C **33**, 130 (1986).
[60] R. Broda *et al.*, Nucl. Phys. A **389**, 366 (1982).
[61] R. Brock *et al.*, Nucl. Phys. A **278**, 45 (1977).
[62] K. Auranen *et al.*, Phys. Rev. C **92**, 039901(E) (2015).
[63] G. Dracoulis *et al.*, Phys. Rev. C **72**, 064319 (2005).
[64] J. M. Lagrange *et al.*, Nucl. Phys. A **530**, 437 (1991).
[65] G. B. Hagemann *et al.*, Nucl. Phys. A **618**, 199 (1997).
[66] W. Nazarewicz, R. Wyss, and A. Johnson, Nucl. Phys. A **503**, 285 (1989).
[67] S. Bouneau *et al.*, Phys. Rev. C **58**, 3260 (1998).
[68] S. Hilaire and M. Girod, Eur. Phys. J. A **33**, 237 (2007).